

11-2020

## **HYPERSPECTRAL PROPERTIES OF DATE PALM TREES (PHOENIX DACTYLIFERA L.)**

Mohamed Ali Saeed Ahmed Al Abdouli

Follow this and additional works at: [https://scholarworks.uaeu.ac.ae/all\\_theses](https://scholarworks.uaeu.ac.ae/all_theses)



Part of the [Agriculture Commons](#), and the [Horticulture Commons](#)

---

### **Recommended Citation**

Ahmed Al Abdouli, Mohamed Ali Saeed, "HYPERSPECTRAL PROPERTIES OF DATE PALM TREES (PHOENIX DACTYLIFERA L.)" (2020). *Theses*. 813.  
[https://scholarworks.uaeu.ac.ae/all\\_theses/813](https://scholarworks.uaeu.ac.ae/all_theses/813)

This Thesis is brought to you for free and open access by the Electronic Theses and Dissertations at Scholarworks@UAEU. It has been accepted for inclusion in Theses by an authorized administrator of Scholarworks@UAEU. For more information, please contact [mariam\\_aljaberi@uaeu.ac.ae](mailto:mariam_aljaberi@uaeu.ac.ae).

United Arab Emirates University

College of Food and Agriculture

Department of Integrative Agriculture

**HYPERSPECTRAL PROPERTIES OF DATE PALM TREES**  
*(PHOENIX DACTYLIFERA L.)*

Mohamed Ali Saeed Ahmed Al Abdouli

This thesis is submitted in partial fulfilment of the requirements for the degree of  
Master of Science in Horticulture

Under the Supervision of Dr. Shyam S. Kurup

November 2020

### **Declaration of Original Work**

I, Mohamed Ali Saeed Ahmed Al Abdouli, the undersigned, a graduate student at the United Arab Emirates University (UAEU), and the author of this thesis entitled “*Hyperspectral Properties of Date Palm Trees (Phoenix dactylifera L.)*”, hereby, solemnly declare that this thesis is my own original research work that has been done and prepared by me under the supervision of Dr. Shyam S. Kurup, in the College of Food and Agriculture at UAEU. This work has not previously been presented or published or formed the basis for the award of any academic degree, diploma or a similar title at this or any other university. Any materials borrowed from other sources (whether published or unpublished) and relied upon or included in my thesis have been properly cited and acknowledged in accordance with appropriate academic conventions. I further declare that there is no potential conflict of interest with respect to the research, data collection, authorship, presentation and/or publication of this thesis.

Student's Signature: \_\_\_\_\_



Date: 18/05/2021

Copyright © 2021 Mohamed Ali Saeed Ahmed Al Abdouli  
All Rights Reserved

## **Advisory Committee**

1) Advisor: Dr. Shyam S. Kurup

Title: Associate Professor

Department of Integrative Agriculture

College of Food and Agriculture

2) Co-advisor: Dr. Mohammed Abdul Muhsen Salem Alyafei

Title: Associate Professor

Department of Integrative Agriculture

College of Food and Agriculture

## Approval of the Master Thesis

This Master Thesis is approved by the following Examining Committee Members:

- 1) Advisor (Committee Chair): Dr. Shyam S. Kurup

Title: Associate Professor

Department of Integrative Agriculture

College of Food and Agriculture

Signature  \_\_\_\_\_

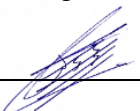
Date 20/05/2021

- 2) Member: Dr. Mohammed Abdul Muhsen Salem Alyafei

Title: Associate Professor

Department of Integrative Agriculture

College of Food and Agriculture

Signature  \_\_\_\_\_

Date 20/05/2021

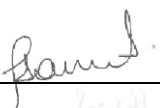
- 3) Member: Dr. Samson Zeray Tesfay

Title: Associate Professor

Department of Horticultural Sciences

College of Agriculture, Engineering and Sciences

University of KwaZulu-Natal, Pietermaritzburg Campus, South Africa

Signature  \_\_\_\_\_

Date 20/05/2021

This Master Thesis is accepted by:

Dean of the College of Food and Agriculture: Professor Bhanu Chowdhary

Signature Bhanu Chowdhary Date 31/05/2021

Dean of the College of the Graduate Studies: Professor Ali Al-Marzouqi

Signature Ali Hassan Date 01/06/2021

Copy \_\_\_\_ of \_\_\_\_

## Abstract

The goal of this study is to classify the Date Palm varieties based on hyperspectral signature technology since it is difficult to identify the Date Palm cultivars without fruits. It will also help to obtain the hyperspectral signature for different types of date palm trees. Moreover, it also assists to determine the wavelength fingerprint of each cultivar and to recommend the best classification protocol differentiating among different cultivars based on spectral signature. Utilizing the Hyperspectral imaging technology precisely on the leaves of different Date Palm cultivars, thus facilitating identification of date palm cultivars without the fruits and make spatial classification. Hyperspectral benefits enable to detect mixtures of materials within same pixel, to identify specific materials with high degree of accuracy, to get some measure of relative abundance based on depth of absorption features and, to produce the quantitative (rather than qualitative) results. For the treatments, in this study, the six cultivars of Date Palm trees (Barhi, Khadrawi, Khenaizi, Khalas, Fard and Helali) were tested. Ten samples for each cultivar from tissue culture were taken and tested considering the same age and identical conditions (control). Later, the samples were analyzed by using the RGB bands. Analyzing the tissue culture samples, the overall results indicate that, each cultivar of Date Palm tree has different spectral signature.

**Keywords:** *Phoenix dactylifera*, hyperspectral imaging, date palm, cultivar, and spectral signature.



## Title and Abstract (in Arabic)

### الخصائص الطيفية لأشجار نخيل التمر

#### الملخص

الهدف من هذه الدراسة هو تصنيف أشجار نخيل التمر على أساس تقنية البصمة من الانبعاث الطيفي لأنه يصعب تحديد أصناف نخيل التمر بدون ثمارها. أيضاً، لتحديد والحصول على بصمة الموج الطيفي للأنواع المختلفة من أصناف نخيل التمر. علاوة على ذلك، لتحديد الطول الموجي لكل صنف من أصناف النخيل والتوصية بأفضل بروتوكول لتمييز الأصناف المختلفة.

والغرض من التصوير الطيفي هو تحديد الأصناف من خلال تحديد بصمة طيفية لكل صنف. كما أن تقنية (Hyperspectral) ستمكننا من تحديد هذه البصمة لكل صنف من أصناف النخيل عن طريق تطبيق هذه التقنية على أوراق النخيل. كما أن هذه التقنية تمتلك دقة عالية في إظهار النتائج.

إن أهمية هذه الدراسة سوف تسهل التعرف على أصناف نخيل التمر بدون اللجوء لرؤية ثمار هذا الصنف أو انتظار موسم الثمار.

في هذه الدراسة، اختبرنا ستة أصناف من أشجار نخيل التمر وهي كالتالي: برحي، خضراوي، خنيزي، خلاص، فرض وهلال. حيث تم اختبار عشر عينات لكل صنف. كما تم اختيار الأصناف من مختبر زراعة الأنسجة من نفس العمر حتى تكون جميعها تحت الظروف المناخية المناسبة.

تم إحضار الأصناف المدروسة من مختبر زراعة الأنسجة لتوحيد العمر وظروف النمو (عينات كونترول).

بعد ذلك تم تحليل البيانات باستخدام تقنية (RGB ANALYSIS) حيث تبين أن لكل صنف من أصناف نخيل التمر بصمة طيفية تختلف عن الصنف الآخر.

**مفاهيم البحث الرئيسية:** أشجار نخيل التمر، التصوير الطيفي الفائق، نخيل التمر، الصنف، التوقيع الطيفي.

## **Acknowledgements**

I would like to express my deepest appreciation to Dr. Shyam S. Kurup, my major supervisor when Dr. Moustafa Fadel left. Without his continuous encouragement, guidance, valuable comments and support this dissertation would not have been possible. I would also like to express my special thanks and deepest appreciation to Dr. Moustafa Fadel, Associate Professor and Dr. Abdelgadir Abuelgasim, Associate Professor, for their valuable suggestions and critical comments on my work. The former was advising me in the conduct of the research from the beginning.

I would also like to express my sincere gratitude to the Dean of Food and Agriculture, to the staff members of the Lab of UAE University, and to the Manager, Engineers and workers of Al Foah Experimental Farm for providing me the precious opportunity to utilize the necessary research equipment and facilities to conduct my research at Al Foah Experimental Farm.

I also would like to express my friend Suheir M. AL Mahadin for teaching me how to use the hyperspectral camera and for her valuable recommendations.

I also would like to express my friend Eng. Ashraf Ali for teaching me how to use and write the references.

I would place my deepest gratefulness to my parents, my family and my friends for their continuous support, advice, and encouragement throughout my academic studies and research.

## **Dedication**

*To my beloved parents, family and friends*

## Table of Contents

Title.....	i
Declaration of Original Work .....	ii
Copyright .....	iii
Advisory Committee .....	iv
Approval of the Master Thesis .....	v
Abstract .....	vii
Title and Abstract (in Arabic) .....	viii
Acknowledgements .....	ix
Dedication .....	x
Table of Contents .....	xi
List of Tables.....	xiii
List of Figures .....	xiv
List of Abbreviations.....	xv
Chapter 1: Introduction .....	1
1.1 Overview .....	1
1.2 Purpose of the Study .....	2
1.3 Background of the Study .....	3
1.4 Research Aim and Objectives .....	7
1.5 The Research will Test the Following Hypothesis .....	7
1.6 Research Significance .....	7
Chapter 2: Review of Literature.....	8
Chapter 3: Materials and Methods .....	24
3.1 Experimental Site.....	24
3.2 Sampling .....	24
3.2.1 Transferring .....	24
3.2.2 Sample Preparation .....	24

3.3 Camera and Lumo Scanner .....	25
3.3.1 Initial Set Up .....	25
3.3.2 Importing and Exporting the Settings .....	30
3.3.3 Run Dark and Run White References .....	30
3.3.4 Defining the Sensor Positions .....	31
3.3.5 Monitoring the Traffic Lights .....	31
3.3.6 Image Capture .....	35
3.4 Analyzing Data .....	37
Chapter 4: Results .....	38
Chapter 5: Discussion .....	56
Chapter 6: Conclusions and Recommendations.....	60
References .....	61
Appendices .....	66

## List of Tables

Table 1: Cumulative Proportion of Reflectance for Barhi, Khenazi, and Khalas .....	51
Table 2: Cumulative Proportion of Reflectance for Khadwri, Fard and Helali.....	53
Table 3: Kolmogorov-Smirnov Normality Test (K-S Test).....	55

## List of Figures

Figure 1: Hyperspectral Imaging Workflow .....	5
Figure 2: Hyperspectral Remote Sensing in Agriculture .....	5
Figure 3: Applications of Hyperspectral Technology .....	6
Figure 4: Adjusting for Settings .....	26
Figure 5: Connect the Camera.....	27
Figure 6: Select the File .....	28
Figure 7: Write the Data of Sample .....	29
Figure 8: Monitor of Traffic Lights .....	32
Figure 9: Prepare the Graph of Sample.....	33
Figure 10: Adjusting of Workflow.....	34
Figure 11: Image Capture.....	35
Figure 12: Save the Image.....	36
Figure 13: Reflectance versus Wavelength of Barhi.....	38
Figure 14: Reflectance versus Wavelength of Khenaizi .....	39
Figure 15: Reflectance versus Wavelength of Khalas .....	39
Figure 16: Reflectance versus Wavelength of Khadrawi.....	40
Figure 17: Reflectance versus Wavelength of Fard .....	40
Figure 18: Reflectance versus Wavelength of Helali.....	41
Figure 19: Reflectance versus Frequency of Barhi .....	42
Figure 20: Reflectance versus Frequency of Khenaizi .....	42
Figure 21: Reflectance versus Frequency of Khalas.....	43
Figure 22: Reflectance versus Frequency of Khadrawi .....	43
Figure 23: Reflectance versus Frequency of Fard.....	44
Figure 24: Reflectance versus Frequency of Helali .....	44
Figure 25: Reflectance versus Frequency of All Cultivar.....	45
Figure 26: Sample Variance.....	47
Figure 27: Standard Deviation .....	48
Figure 28: Reflectance at 705.25 nm .....	49

## **List of Abbreviations**

ASAS	Solid-State Array Spector Radiometer
AVIRIS	Airborne Visible/Infrared Imaging Spectrometer
AVNIR	Airborne Visible and Near Infrared
B	Blue Color
BHC	Binary Hierarchical Classifier
BRD	Bidirectional Reflectance Distribution Function
CIR	Color Infrared
G	Green Color
K-S	Test Kolmogorov-Smirnov Normality Test
LDA	Linear Discriminant Analysis
LSMA	Linear Spectral Mixture Analysis
MPC	Mix to Pure Converter
NDVI	Normalized Difference Vegetation Index
PCA	Principal Component Analysis
PCS	Point Cloud Segmentation Algorithm
R	Red Color
RF	Random Forest
RFCF -FE	Rational Function Curve Fitting Feature Extraction
SDA	Stepwise Discriminant Analysis



## Chapter 1: Introduction

### 1.1 Overview

Date Palm (*Phoenix dactylifera* L.) is a crop of civilization grown in the arid regions of the Arabian Peninsula and the Middle East region. Across the region, people are suffering from a lack of food availability, nutrient deficiency and food security as population growth and land becomes unsuitable for farming (Stringer, 2009). There is a need for fruit crops that can grow in the arid, semi-arid, and saline conditions in the region with limited water and other resources (Arias et al., 2016). In the Arabian and Africa region alone, 100 million date palm trees are grown in one million ha of cropland (Al-Dosary et al., 2016). Cultivation of palm trees are increasing and so is demand for Date fruits. The Food and Agriculture Organization recognizes date palms as a highly important fruit crop when solve the problem of food insecurity and malnutrition and have invested in the research of different aspects of palm fruit cultivation (Arias et al., 2016).

Date palm fruit is a big food source and source of income for local farmer populations in and play significant roles in the Arab economy, and environment in this region. Genetically, date palm is a diploid ( $2n = 2x = 36$ ) chromosomes, date palm is perennial, and monocotyledonous fruit tree belonging to Palmaceae family (Gros-Balthazard et al., 2013). Date palm trees are adapted to arid environment. Thousands of date palm species are found in different regions of date palm growing countries. There are many species of date palm; some of them become dominant in the world market (Chao & Krueger, 2007; Nixon, 1950).

Hyperspectral signature is an important technique that obtains spectral information from an object simultaneously (Serranti et al., 2013). Recently, hyperspectral imaging has been increasingly used in large scale investigation of crops, such as cereal grains, fruits, vegetables, crops and so on (Yao et al., 2013; Huang et al., 2013; Teena et al., 2013). Remote sensing data can prove to be a useful method for detecting plants species (Soroker et al., 2013).

## **1.2 Purpose of the Study**

Remote sensing involves detecting the characteristics of a surface without being in direct contact with the object. There are several benefits of using remote sensing to collect data. Sensors can take measurements of large areas, which are especially useful for large scale agricultural plantations (Soroker et al., 2013). The sensors used are also able to detect factors that are undetectable by human observers, and data collected can be saved and further analyzed by multiple users (Nilsson, 1995). There are multiple factors that can influence the accuracy of the images that result from remote sensing data, and these must be accounted for when conducting analysis (Nilsson, 1995). Hyperspectral signatures were successfully used to detect the leaf blotch on trees according to López-López et al. (2016). Hyperspectral sensors were used to record the reflectance of trees to investigate the possibilities of detecting citrus disease (Sankaran et al., 2013; Li et al., 2014). Hyperspectral signature is a spectral method that can be used to detect plants species. Based on the reflectance of plants at different light spectra it is possible to identify damaged or unhealthy plants (Nilsson, 1995; Clevers & Kooistra, 2012; Mahlein et al., 2010). Hyperspectral devices record the spectral reflectance of a surface at very high spectral resolution – bands of less than 10 nm is typically used (Blackburn, 2007).

Using hyperspectral data, it allows for more accurate estimation of plant biochemical properties, because it is easier to isolate the reflectance of pigments (Blackburn, 2007). The Earth reflect, absorb, transmit and emit electromagnetic energy from the sun. Hyperspectral imaging system has been developed to measure all types of electromagnetic energy as it interacts with objects. A measurement of energy commonly used in remote sensing forestry application is reflected energy such as visible light and near infrared that come from forest canopy surfaces. The amount of energy reflected from these surfaces are usually expressed as a percentage of the amount of energy striking the objects. Across any range of wavelengths, the percent reflectance values for peat swamp forest features can be plotted and compared. Such plots are called “spectral response curves” or “spectral signatures (Mohd, Khali Aziz, & Hamdan, 2011). Recently, the development of small hyperspectral imaging sensors has enabled high spectral and spatial resolution measurements from UAVs. Several pushbroom hyperspectral sensors are used in UAVs (Zarco-Tejada, 2012) (Hruska, 2012) (Büttner & Röser, 2014) (Suomalainen et al., 2014) (Lucieer et al., 2014). The novel hyperspectral cameras operating in the frame format principle offer interesting possibilities for UAV remote sensing by stable imaging geometry and by giving an opportunity to make 3D hyperspectral measurements (Mäkynen et al., 2011). presented the first study with 3D hyperspectral UAV imaging in individual tree-level analysis of bark beetle damage in spruce forests. To the best of the authors’ knowledge, the classification of individual trees using.

### **1.3 Background of the Study**

Hyperspectral imagery from UAVs has not yet been studied. Novel hyperspectral imaging technology based on a variable air gap Fabry–Pérot

interferometer (FPI) operating in the visible to near-infrared spectral range (500–900 nm; VNIR) measurements (Mäkynen et al., 2011) (Honkavaara et al., 2013) was used in this study. The FPI technology makes it possible to manufacture a lightweight, frame format hyperspectral imager operating on the time-sequential principle. The FPI camera can be easily mounted on a small UAV together with an RGB camera, which enables the simultaneous hyperspectral imaging with high spatial resolution photogrammetric point cloud creation (Näsi et al., 2015).

Hyperspectral remote sensing applied to agricultural crops i.e. wheat, paddy, soybean, corn and other crops (Teng et al., 2009). Hyperspectral technique gets more importance in agricultural production applications, Hyperspectral Remote Sensing Applications commonly used in agricultural crops growth monitoring and estimation of crops yield, nutrition diagnosis and fertilizer, agricultural product quality, safety and diseases testing and many other aspects currently this application research in the field of agriculture of hyperspectrum focuses on the agriculture crop and products, including fruits, livestock products and economic crops (Wang et al., 2016).

With a hyperspectral camera, the light is captured through a lens and split into different spectral lengths by a dispersive element such as a prism or a diffraction grating. Also possible is a recording of different wavelengths at different positions in the FOV. The heart of the MHSI camera is a CCD or CMOS detector array that reads out the information inherent to the captured light (Figure 1).

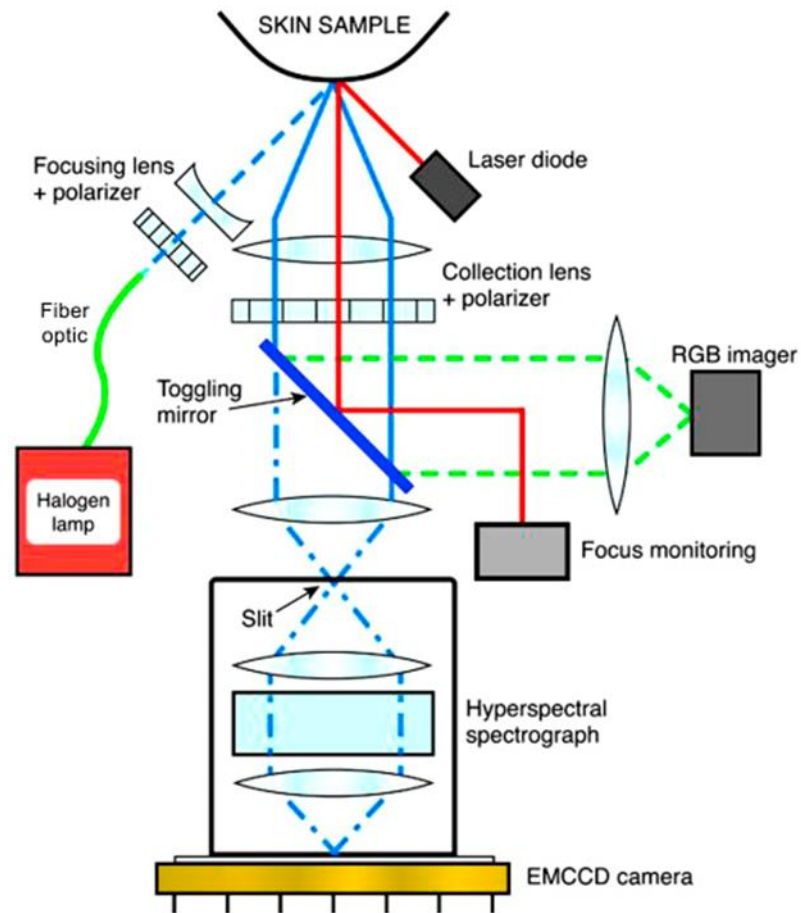


Figure 1: Hyperspectral Imaging Workflow

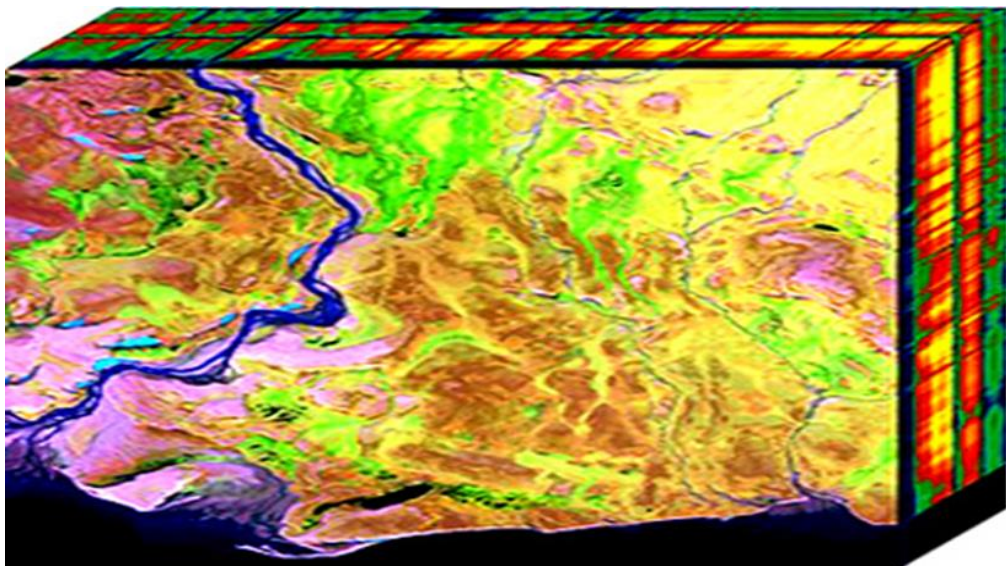


Figure 2: Hyperspectral Remote Sensing in Agriculture

Date palm is an important cash crop in Middle East and African countries with limited water availability their hardiness in tough conditions. This research has shown that thermal, multispectral, and hyperspectral remote sensing imagery can provide insight into the health of date palm plantations as in Figure 2, 3. The study used to available thermal, hyperspectral, Light detection and ranging (LiDAR) and visual red, green blue (RGB) images to find the possibilities of assessing date palm health at two “levels”; block level and individual tree level. Test blocks were defined into assumed healthy and unhealthy classes and thermal and height data were extracted and compared. Due to distortions in the hyperspectral imagery, this data was only used for individual tree analysis.

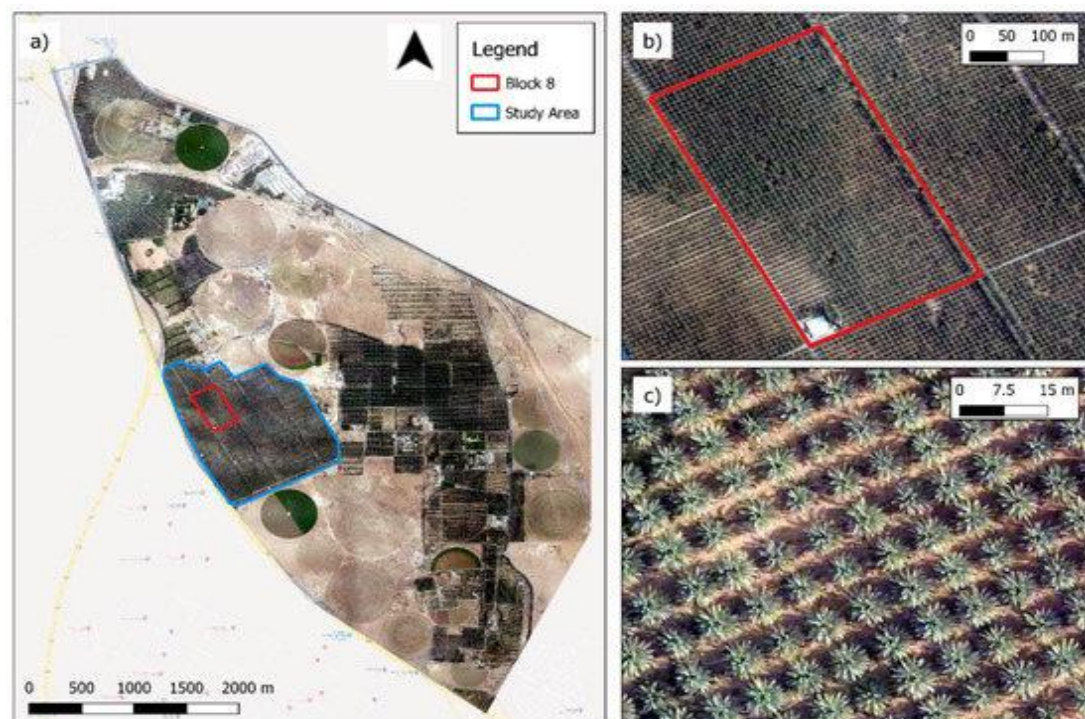


Figure 3: Applications of Hyperspectral Technology

## **1.4 Research Aim and Objectives**

The aim of this study is to test the use of high-resolution photogrammetric point clouds together with hyperspectral UAV imaging in individual tree detection and classification in particular, the data processing challenges in a real forest environment will be studied and the importance of different spectral and structural features in tree species classification will be assessed.

The major objectives of the research are:

1. To classify date palm trees based on hyperspectral signature technology because it is difficult to identify the date palm cultivars without fruits.
2. Hyperspectral imaging to identify the cultivars by determining the spectral signature for each cultivar.

## **1.5 The Research will Test the Following Hypothesis**

This study will be able to classify date palm trees on hyperspectral signature technology to identify date palm cultivars without fruit and to determine the spectral signature for each cultivar for precise identification. The study will be successful utilizing this technology on leaves of different date Palm cultivars.

## **1.6 Research Significance**

Classifying date palm trees based on hyperspectral signature technology will be helpful to obtain the hyperspectral signature for different type of date palm trees and to determine wavelength fingerprint of each cultivar. Also, to recommend the best classification protocol to differentiate among different cultivars based on spectral signature.

## Chapter 2: Review of Literature

Hyperspectral technology imaging spectrometry technology is one of the important leading research fields of remote sensing. Since the first imaging spectrometer was produced in 1983, in less than 20 years. Hyperspectral remote sensing technology has been successfully applied in many fields and shown great potential and bright prospects. However, the research on processing and applications of Hyperspectral remote sensing data has fallen far behind the research on sensors. Research on processing, analysis and information extraction of Hyperspectral data should be strengthened to determine more useful information, make full use of the advantage and potential of Hyperspectral remote sensing technology, and promote the development of new and important technology (Jiang et al., 2004).

According to work carried out by Thenkabail et al. (2004) where they determine the best Hyperspectral wavebands in the study of date palms and agricultural crops over the spectral range of 400 – 2500 nm and also assessed the date palms and agricultural crop classification accuracies achievable using the various combinations of the best Hyperspectral narrow wavebands. The Hyperspectral data were gathered for date palms, shrubs, grasses, weeds, and agricultural crop species from the four eco-regions of African savannas using a 1-nm-wide hand-held spectroradiometer but was aggregated to 10-nm-wide bandwidths to match the first space borne Hyperspectral sensor, Hyperion. After accounting for atmospheric widows and/or areas of significant noise, a total of 168 narrow bands in 400 – 2500 nm was used in the analysis. Rigorous data mining techniques consisting of principal component analysis (PCA), lambda–lambda 2 models (LL R 2 M), stepwise discriminant analysis (SDA), and derivative



greenness vegetation indices (DGVI) established 22 optimal bands (in 400 – 2500 nm spectral range) that best characterize and classify vegetation and agricultural crops. Overall accuracies of over 90% were attained when the 13 – 22 best narrow bands were used in classifying vegetation and agricultural crop species. Beyond 22 bands, accuracies only increase marginally up to 30 bands. Accuracies become asymptotic or near zero beyond 30 bands, rendering 138 of the 168 narrow bands redundant in extracting vegetation and agricultural crop information. Relative to Landsat Enhanced Thematic Mapper plus (ETM+) broad bands, the best Hyperspectral narrow bands provided an increased accuracy of 9 – 43% when classifying shrubs, weeds, grasses, and agricultural crop species.

According to Chao et al. (2007) the Palm trees are a family (Arecaceas) of plants with hundreds of species. Most economically important species are date palm (*Phoenix dactylifera* L.), coconut palm (*Cocos nucifera*), and oil palm (*Elaeis guineensis*). Being monocotyledons, palm trees show distinct differences of the wood structure compared to common wood species. This study aimed to evaluate the anatomical properties ‘Tadmament’ cultivar of date palm wood such as density, frequency, diameter, and area of vascular bundles (VB) in stem sections/zones (from the peripheral to the inner zone), and at two different stem heights (Top and bottom of the stem). The results indicated that the density and frequency of vascular bundles increase from the inner to the peripheral zones of the stem, thus the diameter and area of VB decrease from the first to the third zones. The density of VB in peripheral zone also decreases from the bottom to the top of the stem. In addition, it has been increased in the central and inner zones. In the peripheral and central zones, the VB are numerous and smaller in diameter. The inner zone is the broadest; the bundles reach their highest diameter. The fiber tissue percent is higher in the peripheral and central zones (48.5% / 44.5%, at the

bottom and top of stem respectively) than in the inner zone (9% / 11%, at the bottom and top of stem respectively). The results of this study will be used to calculate density of sap flux, also to develop the injection techniques to fight the red date palm weevil (*Rhynchophorus ferrugineus*). Results for coconut and oil palm are different; the vascular bundles have a constant size throughout the central cylinder.

Chao and Krueger (2007) studied the date palm (*Phoenix dactylifera L.*) is one of the oldest fruit crops grown in the arid regions of the Arabian Peninsula, North Africa, and the Middle East. The most probable area of origin of the date palm was in or near what is now the country of Iraq, but date cultivation spread to many countries starting in ancient times. Dates are a major food source and income source for local populations in the Middle East and North Africa, and play significant roles in the economy, society, and environment in these areas. In addition to serving directly as a food source, dates are packed and processed in several ways, and other parts of the tree are used for various purposes. The date palm is a diploid, perennial, dioecious, and monocotyledonous plant adapted to arid environments. It has unique biological and developmental characteristics that necessitate special propagation, culture, and management techniques. Thousands of date palm cultivars and selections exist in different date-growing countries. Different genetic marker systems have been used to study genetic relationships among date palm cultivars. The long-life cycle, long period of juvenility, and dioecism of date palms make breeding challenging. Worldwide date production has grown from 1,809,091 t in 1962 to 6,924,975 t in 2005. Worldwide date production will continue to grow, especially in the Middle East, despite current and future challenges.

Siddiq and Greiby (2014) studied that the date palm is grown in over 30 countries around the world; in recent years, date fruit has gained significant importance in global commerce. During the last two decades, global production of dates has more than doubled. Most date palm-growing areas are in developing or underdeveloped countries where date fruit is considered a primary food crop, thus playing a major role in the nutritional status of these communities. Marketing of dates involves various operations through the value-chain, e.g., harvesting, cleaning, grading, packaging, processing, and transportation/shipment to local or export markets. Some of the major challenges confronting date fruit production and commerce are issues related to postharvest handling technologies, use of appropriate processing and packaging technologies, food safety aspects, and quality assurance. This chapter provides an overview of production, harvesting and GAPs/GMPs, postharvest handling and storage, processing, processed products/by-products, nutritional profile, bioactive compounds, and health benefits of dates.

Majidi Heravan et al., (2002) study was carried out to investigate the morphological and anatomical aspects of somatic embryogenesis in date palm. Lateral bud and shoot tip explants excised from young offshoots were cultured on MS medium with 2,4-D. Somatic embryogenesis was induced by transferring the calli produced on the same medium without hormones. Microtome sectioning of paraffin-embedded specimens was carried out using the callus tissue and its differentiated structures. The sections were stained with safranin and fast green. Observation of three-celled proembryos with the longitudinal and oblique division of the top cell, which in later stages results in wedge-like cell(s), supports the ASTERAD type of embryogenesis in date palm. Polyembryonic structures were raised from the embryonic callus formed in

different regions of both the proembryos and germinating embryos and the secondary embryos formed directly from primary embryos.

Chao and Krueger (2007) studied that the *Phoenix dactylifera*, commonly known as date or date palm is a flowering plant species in the palm family, Arecaceae, cultivated for its edible sweet fruit. Although its exact place of origin is uncertain because of long cultivation, it probably originated from the Fertile Crescent region straddling between Egypt and Mesopotamia. Krueger and Robert (2007) studied the species is widely cultivated across Northern Africa, the Middle East, the Horn of Africa and South Asia and is naturalized in many tropical and subtropical regions worldwide. *P. dactylifera* is the type species of genus *Phoenix*, which contains 12–19 species of wild date palms, and is the major source of commercial production.

Jusoff and Pathan (2009) studied that the date trees typically reach about 21–23 meters (69–75 ft) in height, growing singly or forming a clump with several stems from a single root system. Date fruits (dates) are oval-cylindrical, 3 to 7 centimeters (1.2 to 2.8 in) long, and about 2.5 centimeters (0.98 in) in diameter, ranging from bright red to bright yellow in colour, depending on variety. At about 61–68 percent sugar by mass when dried, dates are a very sweet fruit.

NPR organization (2015) reported that the Fossil records show that the date palm has existed for at least 50 million years. Dried date, peach, and apricot from Lahun, Fayum, Egypt.

Tengberg (2012) studied that the dates have been a staple food of the Middle East and the Indus Valley for thousands of years. They are believed to have originated around what is now Iraq. There is archaeological evidence of date cultivation in Mehrgarh around 7000 BCE, a Neolithic civilization in what is now western Pakistan and in eastern Arabia between 5530 and 5320 calBC. and have been

cultivated since ancient times from Mesopotamia to prehistoric Egypt. The ancient Egyptians used the fruits to make date wine, and ate them at harvest. Evidence of cultivation is continually found throughout later civilizations in the Indus Valley, including the Harappan period of 2600 to 1900 BCE. The ancient Hebrews made the fruit into wine, vinegar, bread, and cakes, also using the fruit stones to fatten livestock and the wood to make utensils.

Nilsson (1995) studied that the germination of 200 years old seeds of *Phoenix dactylifera* from Judean desert archaeological site provide a unique opportunity to study the Judean date palm, described in antiquity for the quality, size, and medicinal properties of its fruit, but lost for centuries. Microsatellite genotyping of germinated seeds indicates that exchanges of genetic material occurred between the Middle East (eastern) and North Africa (western) date palm gene pools, with older seeds exhibiting a more eastern nuclear genome on a gradient from east to west of genetic contributions. Ancient seeds were significantly longer and wider than modern varieties, supporting historical records of the large size of the Judean date. These findings, in accord with the region's location between east and west date palm gene pools, suggest that sophisticated agricultural practices may have contributed to the Judean date's historical reputation. Given its exceptional storage potentialities, the date palm is a remarkable model for seed longevity research.

Taxonomic Tree. ENH1212.

Domain: Eukaryota

Kingdom: Plantae

Phylum: Spermatophyta

Subphylum: Angiospermae

Class: Monocotyledonae

Order: Arecales

Family: Arecaceae

Genus: Phoenix

Species: *Phoenix dactylifera*

Rajabi and Ghassemian (2015) studied a variety of feature reduction methods that have been developed by using spectral and spatial domains. In these studies, a feature extracting technique was proposed based on rational function curve fitting. For each pixel of a Hyperspectral image, a specific rational function approximation was developed to fit the spectral response curve of that pixel. Coefficients of the numerator and denominator polynomials of these functions were considered as new extracted features. This new technique is since the sequence discipline - ordinance of reflectance coefficients in spectral response curve - contains some information which has not been considered by other statistical analysis-based methods, such as Principal Component Analysis (PCA) and Linear Discriminant Analysis (LDA) and their nonlinear versions. Also, they showed that naturally different curves can be approximated by rational functions with equal form, but different amounts of coefficients. Maximum likelihood classification results demonstrated that the Rational Function Curve Fitting Feature Extraction (RFCF -FE) method provides better classification accuracies compared to competing feature extraction algorithms. The method, also, had the ability of lossy data compression. The original data was reconstructed using the fitted curves. In addition, the proposed algorithm has the possibility to be applied to all pixels of image individually and simultaneously, unlike to PCA and other methods which need to know whole data for computing the transform matrix.

Teena et al. (2013) studied that the early stages of microbial infection in date palm fruits are difficult to detect by the presently used manual sorting technique. The potential of Hyperspectral imaging technique to detect fungal contamination of edible date fruits was investigated in their study. The samples were treated as three groups: untreated control (UC), sterile control (SC) (surface sterilized, rinsed, and dried) and inoculated samples (IS) (surface sterilized, rinsed, dried and inoculated). Hyperspectral images of control samples and *Aspergillus flavus* inoculated date fruits were acquired using an area scan Hyperspectral imaging system from 75 image slices at 10 nm intervals between 960 and 1700 nm after every 48 h of inoculation for 10 days. The top four most significant wavelengths corresponding to the highest factor loadings of the first principal components (PC) were selected and used for feature extraction. A total of 64 features (16 features from each selected wavelength) were extracted and applied in the statistical classifications (linear discriminant analysis (LDA) and quadratic discriminant analysis (QDA)). The classification accuracies for IS were compared with UC and SC separately using six-class model (control, infected day 2, day 4, day 6, day 8 and day 10), two-class model (control vs infected (all stages of infection together)) and pair-wise model (control vs each stage of infection). The mean classification accuracy (LDA and QDA) of IS was 91.5%, 91.0% and 99.0% for six-class model, two-class model, and pairwise-model, respectively while comparing with SC. Similarly, it was 92.4%, 100.0% and 99.6% for six-class model, two-class model, and pairwise-model, respectively while comparing with UC. In general, quadratic discriminant analysis yielded better accuracy than linear discriminant analysis in all the classification models tested. Further work is required to test this technique for other species of fungal infections and its effect on the chemical composition of different date fruit varieties.

Shen and Cao (2017) reported that the accurate classification of tree-species is essential for sustainably managing forest resources and effectively monitoring species diversity. In their study, they used simultaneously acquired Hyperspectral and LiDAR data from LiCHy (Hyperspectral, LiDAR and CCD) airborne system to classify tree-species in subtropical forests of southeast China. First, each individual tree crown was extracted using the LiDAR data by a point cloud segmentation algorithm (PCS) and the sunlit portion of each crown was selected using the Hyperspectral data. Second, different suites of Hyperspectral and LiDAR metrics were extracted and selected by the indices of Principal Component Analysis (PCA) and the mean decrease in Gini index (MDG) from Random Forest (RF). Finally, both Hyperspectral metrics (based on whole crown and sunlit crown) and LiDAR metrics were assessed and used as inputs to Random Forest classifier to discriminate five tree-species at two levels of classification. The results showed that the tree delineation approach (point cloud segmentation algorithm) was suitable for detecting individual tree in this study (overall accuracy = 82.9%). The classification approach provided a relatively high accuracy (overall accuracy > 85.4%) for classifying five tree-species in the study site. The classification using both Hyperspectral and LiDAR metrics resulted in higher accuracies than only Hyperspectral metrics (the improvement of overall accuracies = 0.4–5.6%). In addition, compared with the classification using whole crown metrics (overall accuracies = 85.4–89.3%), using sunlit crown metrics (overall accuracies = 87.1–91.5%) improved the overall accuracies of 2.3%. The results also suggested that fewer of the most important metrics can be used to classify tree-species effectively (overall accuracies = 85.8–91.0%).

Foody et al. (2006) reported that the Statistical classification of Hyperspectral data is challenging because the inputs are high in dimension and represent multiple



classes that are sometimes quite mixed, while the amount and quality of ground truth in the form of labeled data is typically limited. The resulting classifiers are often unstable and have poor generalization. This work investigated two approaches based on the concept of random forests of classifiers implemented within a binary hierarchical multi classifier system, with the goal of achieving improved generalization of the classifier in analysis of Hyperspectral data, particularly when the quantity of training data is limited. A new classifier was proposed, that incorporates bagging of training samples and adaptive random subspace feature selection within a binary hierarchical classifier (BHC), such that the number of features that is selected at each node of the tree is dependent on the quantity of associated training data. Results are compared to a random forest implementation based on the framework of classification and regression trees.

For both methods, classification results obtained from experiments on data acquired by the National Aeronautics and Space Administration (NASA) Airborne Visible/Infrared Imaging Spectrometer instrument over the Kennedy Space Center, Florida, and by Hyperion on the NASA Earth Observing 1 satellite over the Okavango Delta of Botswana are superior to those from the original best basis BHC algorithm and a random subspace extension of the BHC.

Govender et al. (2006) reported that the multispectral imagery has been used as the data source for water and land observational remote sensing from airborne and satellite systems since the early 1960s. Over the past two decades, advances in sensor technology have made it possible for the collection of several hundred spectral bands. This is commonly referred to as Hyperspectral imagery. This review details the differences between multispectral and Hyperspectral data; spatial and spectral

resolutions and focuses on the application of Hyperspectral imagery in water resource studies and, in particular the classification and mapping of land uses and vegetation.

Tarabalka et al. (2011) studied that the high number of spectral bands acquired by Hyperspectral sensors increase the capability to distinguish physical materials and objects, presenting new challenges to image analysis and classification. This work presented a novel method for accurate spectral-spatial classification of Hyperspectral images. The proposed technique consists of two steps. In the first step, a probabilistic support vector machine pixel wise classification of the Hyperspectral image was applied. In the second step, spatial contextual information was used for refining the classification results obtained in the first step. This is achieved by means of a Markov random field regularization. Experimental results were presented for three Hyperspectral airborne images and compared with those obtained by recently proposed advanced spectral-spatial classification techniques. The proposed method improves classification accuracies when compared to other classification approaches.

Zarco-Tejada et al. (2005) showed that the traditional remote sensing methods for yield estimation rely on broadband vegetation indices, such as the Normalized Difference Vegetation Index, NDVI. Despite demonstrated relationships between such traditional indices and yield, NDVI saturates at larger leaf area index (LAI) values, and it is affected by soil background. The results obtained with several new narrow-band Hyperspectral indices calculated from the Airborne Visible and Near Infrared (AVNIR) Hyperspectral sensor flown over a cotton (*Gossypium hirsutum* L.) field in California (USA) collected over an entire growing season at 1-m spatial resolution. Within-field variability of yield monitor spatial data collected during harvest was correlated with Hyperspectral indices related to crop growth and canopy structure, chlorophyll concentration, and water content. The time-series of indices calculated

from the imagery were assessed to understand within-field yield variability in cotton at different growth stages. A K means clustering method was used to perform field segmentation on Hyperspectral indices in classes of low, medium, and high yield, and confusion matrices were used to calculate the kappa ( $\kappa$ ) coefficient and overall accuracy. Structural indices related to LAI [Renormalized Difference Vegetation Index (RDVI), Modified Triangular Vegetation Index (MTVI), and Optimized Soil-Adjusted Vegetation Index (OSAVI)] obtained the best relationships with yield and field segmentation at early growth stages. Hyperspectral indices related to crop physiological status [Modified Chlorophyll Absorption Index (MCARI) and Transformed Chlorophyll Absorption Index (TCARI)] were superior at later growth stages, close to harvest. From confusion matrices and class analyses, the overall accuracy (and kappa) of RDVI at early stages was 61% ( $\kappa = 0.39$ ), dropping to 39% ( $\kappa = 0.08$ ) before harvest. The MCARI chlorophyll index remained sensitive to within-field yield variability at late pre-harvest stage, obtaining overall accuracy of 51% ( $\kappa = 0.22$ ).

Hirano et al. (2003) reported that the Data acquired by the Airborne Visible/Infrared Imaging Spectrometer (AVIRIS) with 224 bands, each with 0.01- $\mu\text{m}$  spectral resolution and 20-meter spatial resolution, were used to produce a vegetation map for a portion of Everglades National Park, Florida, USA. The vegetation map was tested for classification accuracy with a pre-existing detailed GIS wetland vegetation database compiled by manual interpretation of 1:40,000-scale color infrared (CIR) aerial photographs. Although the accuracy varied greatly for different classes, ranging from 40 percent for scrub red mangroves (*Rhizophora mangle*) to 100 percent for spike rush (*Eleocharis cellulose*) prairies, the Everglades communities generally were successfully identified, averaging 66 percent correct for all classes. In addition, the

Hyperspectral image data proved suitable for detecting the invasive exotic species lather leaf (*Colubrina asiatica*) that is sometimes difficult to differentiate on aerial photographs. The findings from this study have implications for operational uses of space borne Hyperspectral image data that are now becoming available. Practical limitations of using such image data for wetland vegetation mapping include inadequate spatial resolution, complexity of image processing procedures, and lack of stereo viewing.

The work carried out by Esau et al. (2006), showed that the Leaf traits and physiological performance govern the amount of light reflected from leaves at visible and infrared wavebands. Information on leaf optical properties of tropical trees is scarce. In their experiment, they examined leaf reflectance of Mesoamerican trees for three applications: to compare the magnitude of within- and between-species variability in leaf reflectance, to determine the potential for species identification based on leaf reflectance, and to test the strength of relationships between leaf traits (chlorophyll content, mesophyll attributes, thickness) and leaf spectral reflectance. Within species, shape and amplitude differences between spectra were compared within single leaves, between leaves of a single tree, and between trees. They also investigated the variation in a species' leaf reflectance across sites and seasons. Using forward feature selection and pattern recognition tools, species classification within a single site and season was successful, while classification between sites or seasons was not. The implications of variability in leaf spectral reflectance were considered in light of potential tree crown classifications from remote airborne or satellite-borne sensors. Species classification is an emerging field with broad applications to tropical biologists and ecologists, including tree demographic studies and habitat diversity assessments. Mountrakis et al. (2011) studied the wide range of methods for analysis of airborne-

and satellite-derived imagery continues to be proposed and assessed. SVMs are particularly appealing in the remote sensing field due to their ability to generalize well even with limited training samples, a common limitation for remote sensing applications. However, they also suffer from parameter assignment issues that can significantly affect obtained results.

Sandmeier et al. (1998) reported a new approach for deriving vegetation canopy structural characteristics from Hyperspectral bidirectional reflectance distribution function (BRDF) data. The methodology is based on the relationship between spectral variability of BRDF effects and canopy geometry. Tests with data acquired with the Advanced Solid-State Array Spector radiometer (ASAS) over Canadian boreal forests during the BOREAS campaign show that vegetation structural characteristics can be derived from the spectral variability of BRDF effects. In addition, the incorporation of both BRDF effects and Hyperspectral resolution data substantially improve the classification accuracy. Best classification results are obtained when Hyperspectral resolution and BRDF data are combined, but the improvement is not consistent for all classes. For example, adding BRDF information to Hyperspectral data increases the overall classification accuracy for a six-class fen site from 37.8% to 44.7%. The addition, however, reduces the accuracy for the jack pine class from 43.6% to 28.8%. These new findings provide evidence for improved capabilities for applications of MISR and MODIS data. The spectral resolution of MODIS is expected to be sufficient to derive canopy structural information based on the spectral variability of BRDF effects, and for MISR a significant improvement of classification accuracies can be anticipated from the combination of nadir reflectance and off-nadir data.

The work carried out by Key et al. (2001) found that the Multi temporal, small-format 35-mm aerial photographs were combined in a co-registered database to determine the relative value of spectral and phenological information for over story tree crown classification of digital images of the Eastern Deciduous Forest. A one-hectare study site, located in a second-growth forest 15 km east of Morgantown, West Virginia, USA, was photographed from a light aircraft nine times from May to October 1997 using both true-color and false-color infrared film. Using this imagery, differences in the spectral properties and timing of phenologic events between tree species made it possible to discriminate four tree species, namely *Liriodendron tulipifera*, *Acer rubrum*, *Quercus rubra*, and *Quercus alba*, which made up nearly 99% of the trees at this study site. Optimally timed photography acquired during peak autumn colors provided the best single date of imagery, while photography from spring leaf-out was the second best. The best individual image band for tree species discrimination was the blue band. Classifications using all four spectral bands (blue, green, red, and infrared) and four dates (05/23/97, 06/23/97, 10/11/97, and 10/30/97) provided the best classification accuracies. Variable canopy illumination made digital classification of individual trees complex. A Likelihood Ratio test confirmed that the number of spectral bands included in the classification procedure (spectral resolution) and the number of dates (temporal resolution) significantly influenced the ability to identify tree species correctly. This study suggests that although multispectral data appear to be more valuable than multitemporal data, it may be possible to compensate for the limited spectral resolution of planned high-resolution sensors by combining multiple dates of low spectral resolution images.

Jusoff and Pathan (2009). reported a preamble step for developing an approach for mapping individual oil palm trees from airborne hyperspectral imaging. The study

generally describes airborne hyperspectral sensors in different fields particularly in agriculture by comparing and analyzing their uniqueness for different applications. The emphasis is on the image processing in identifying and mapping of the individual oil palm trees with the utilization of image histogram to examine the RGB bands. An algorithm was designed to discover the involvement of different materials in a single mixed pixel and converting it into a pure pixel. The techniques employ in this connection are Linear Spectral Mixture Analysis (LSMA), Mix to Pure Converter (MPC) and Euclidean Norm.

## **Chapter 3: Materials and Methods**

### **3.1 Experimental Site**

The experiments were conducted in the Building E2 (laboratory of food science) of College of Food and Agriculture United Arab Emirates University where hyperspectral camera (Specimen, Spectral Imaging Oy Ltd) was used to take photos for the leaf samples. Also, leaf sample has been collected from tissue culture laboratory in Al foah research farm, College of Food and Agriculture United Arab Emirates University. It lies in the co-ordinate latitude and longitude of  $24.2191^{\circ}$  N and  $55.7146^{\circ}$  E.

### **3.2 Sampling**

Leaf samples were collected from Al Foah in the same day and time, samples for each type were taken as triplets from ten different pots in the same age (10 leaf for each verity).

#### **3.2.1 Transferring**

Samples were transferred to lab 3 in black bags to avoid any surrounding effect.

#### **3.2.2 Sample Preparation**

Samples were taped from edges to a clean white sheet. There is no chemical analysis using to avoid and effects on the leaves.



### **3.3 Camera and Lumo Scanner**

The Lumo Scanner software has been used to control the hyperspectral camera and the scanner (Specim, Spectral Imaging Oy Ltd), the software has a built-in scripting and sequential workflow engine controlling all the steps and automation to be performed for each measurement.

The work started by initial camera calibration:

Initial set up.

1. Adjust for setting camera parameters and workflow.
2. Capture for image acquisition.

#### **3.3.1 Initial Set Up**

The License activation (Specim\_QtRuntime\_redist\_setup\_5.4.1.exe. 5.4.1), and the other initial set up steps were carried out previously by the food science department and the system was ready to use from the start of this experiment.

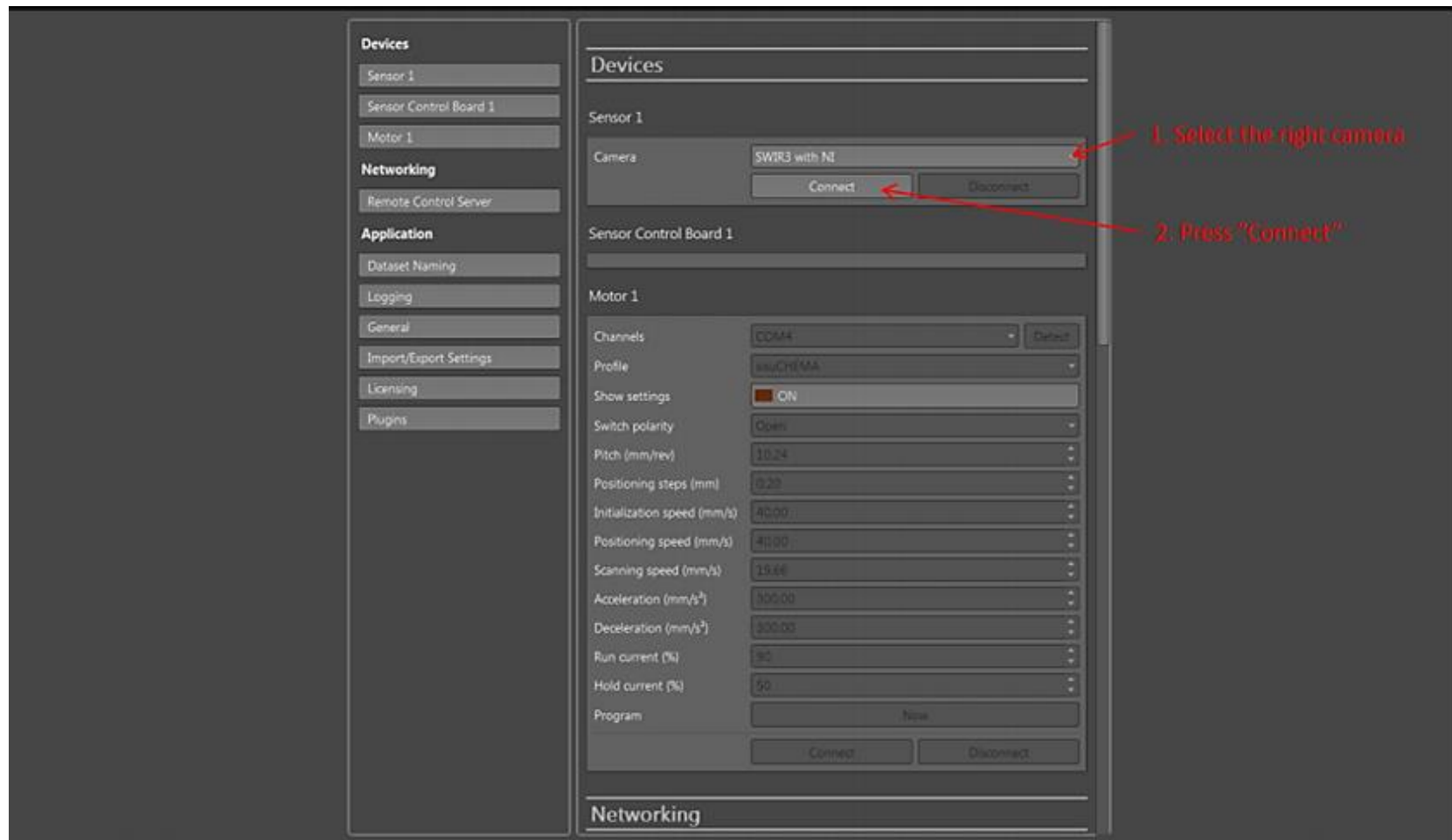


Figure 4: Adjusting for Settings

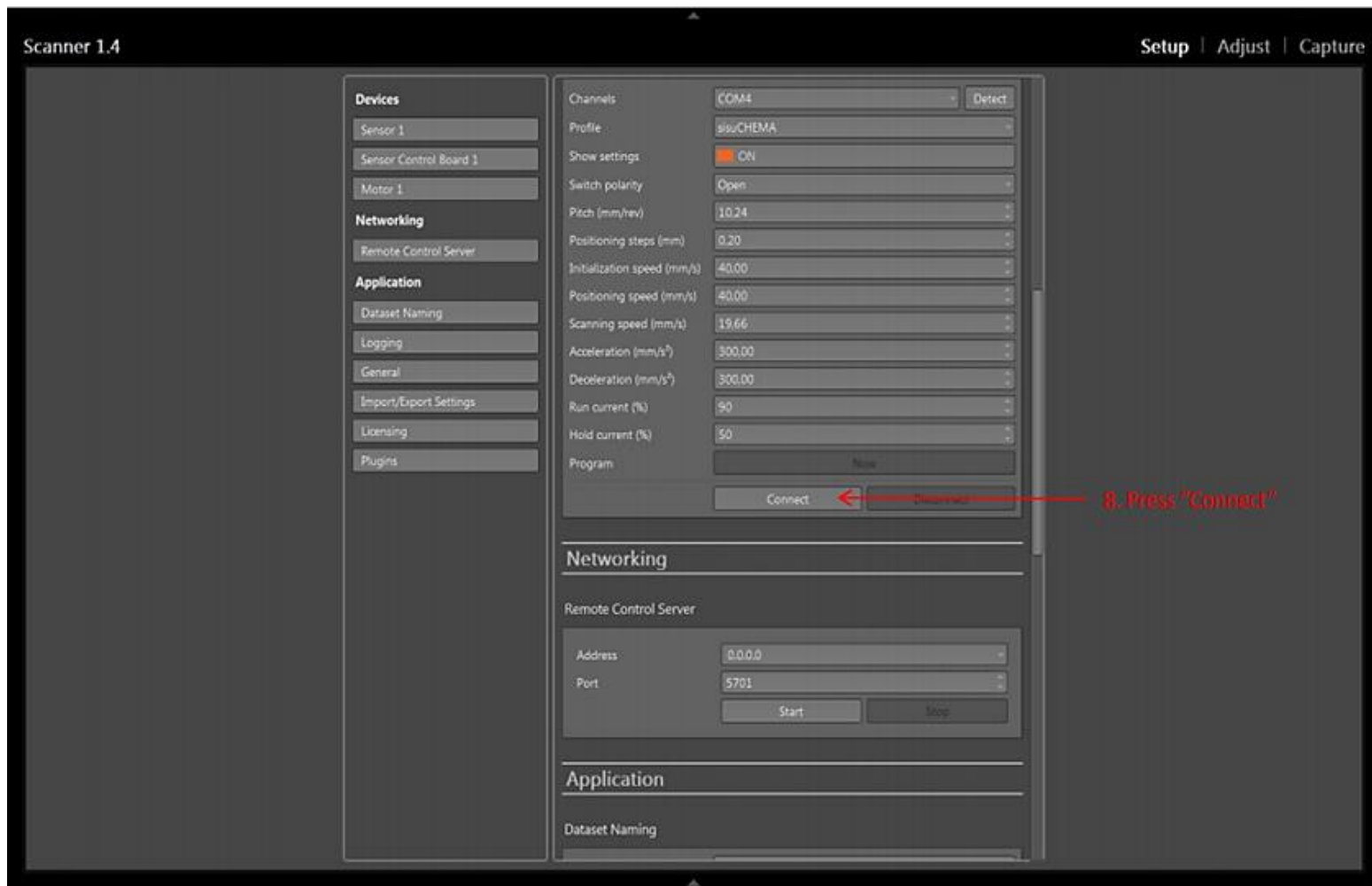


Figure 5: Connect the Camera

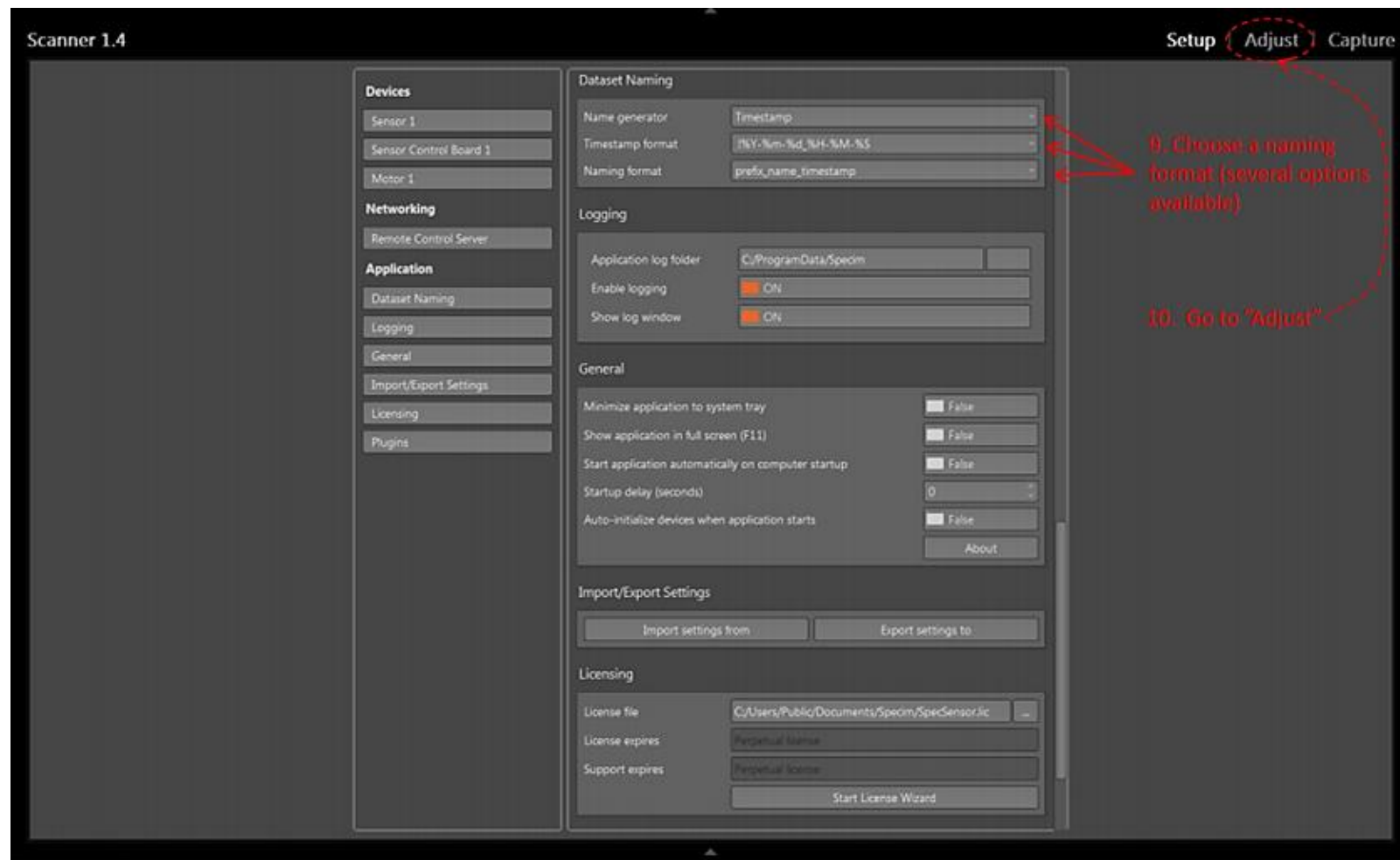


Figure 6: Select the File

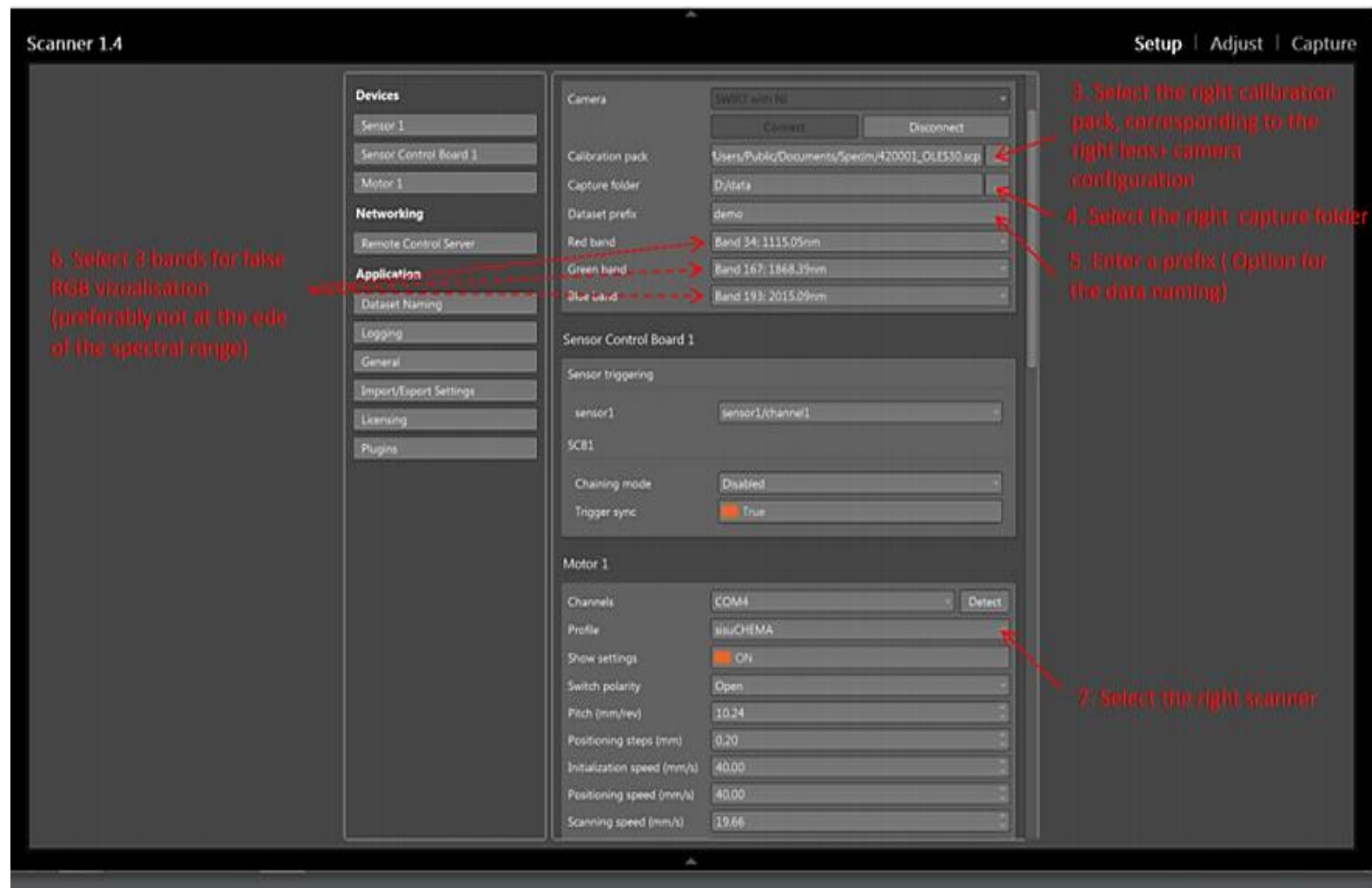


Figure 7: Write the Data of Sample

### 3.3.2 Importing and Exporting the Settings

To make sure, the samples were run with the same adjusting parameters from the Setup View in the Import/export settings group.

- a. Click 'Export settings to button, then after entering the file name for the exported settings file, and the folder location is selected and the 'Save' button is pressed and it is ensured to get the message showing "Settings exported successfully".
- b. Each time when the camera is used it was set with the same importing settings and then the settings file is selected which is previously exported.
- c. After selecting the settings file, Restart button must be clicked to continue with the import.

### 3.3.3 Run Dark and Run White References

To acquire and apply the captured or defined dark and white current level.

Pixels may not be entirely dark, even when no light reaches the sensor. This is called the dark current level. To correct the image, dark current is subtracted from the data. The dark current reference can be acquired from the sensor or defined with many options, Shutter, Constant, Thermal Calibrator, Manual, or Scanner option.

The selected Shutter option includes the dedicated workflow, the sensor's shutter closes, and 100 frames (are acquired). The frames are averaged to a single dark reference frame, and the shutter re-opens (Each pixel has its own measured dark current value).

The white reference specifies the maximum pixel value for all pixels (Together with the dark reference, the white reference is used for). The white reference can be acquired from the sensor or defined with one of the Constant, Manual, Thermal Calibrator, Scanner, or Radiometric options.

Next, the selection of Scanner option is done. The scanner moves to the white reference start position, and 100 frames are acquired. The frames are averaged to a single white reference frame, and the scanner retraces. Each pixel in the frame has its own measured maximum value.

### **3.3.4 Defining the Sensor Positions**

It is so important to define the positions and acquisition methods of the acquisition target, the white reference, and the samples, because the scanner first accelerates, then runs at constant speed over the target range, until decelerates and stops. If the start or stop position is too close to the end of the scanner range, there will be no room to accelerate or decelerate. In this case, running the workflow will fail.

Move the scanner using the Motor Remote Control so that the focusing grid is in view.

Move the scanner to the start of the white reference.

Press the Set button of the white start field.

Move the scanner to the end of the white reference.

Press the Set button of the white end field.

Repeat steps for the start and end of the sample (Target) positions.

Press the Go button at each position and verify that the desired positions have been set.

### **3.3.5 Monitoring the Traffic Lights**

The traffic lights display information about the current system status, that include hardware status information, received data, and undefined application parameters etc., so to start it is ensured that no red boxes are shown in the traffic lights.

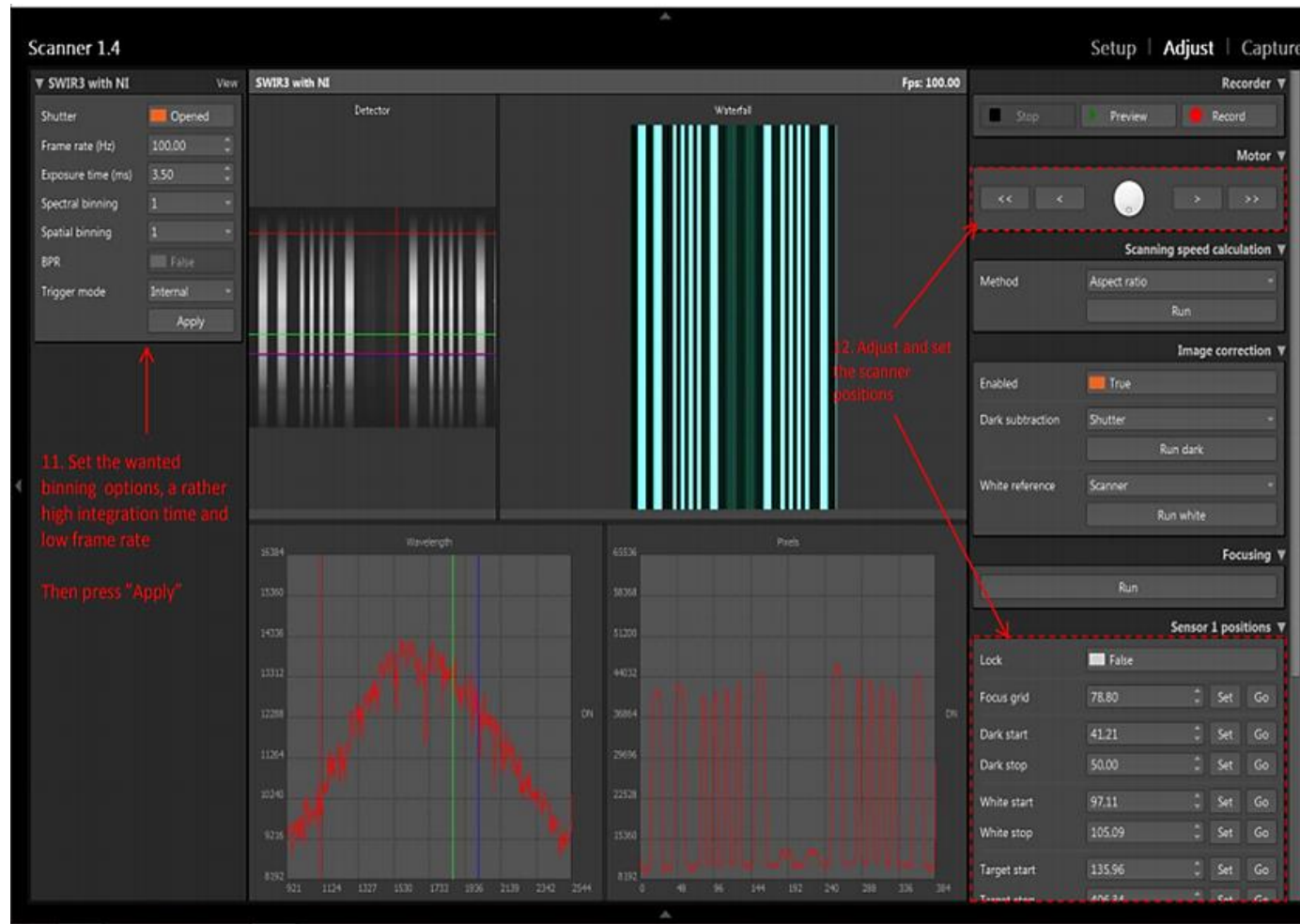


Figure 8: Monitor of Traffic Lights



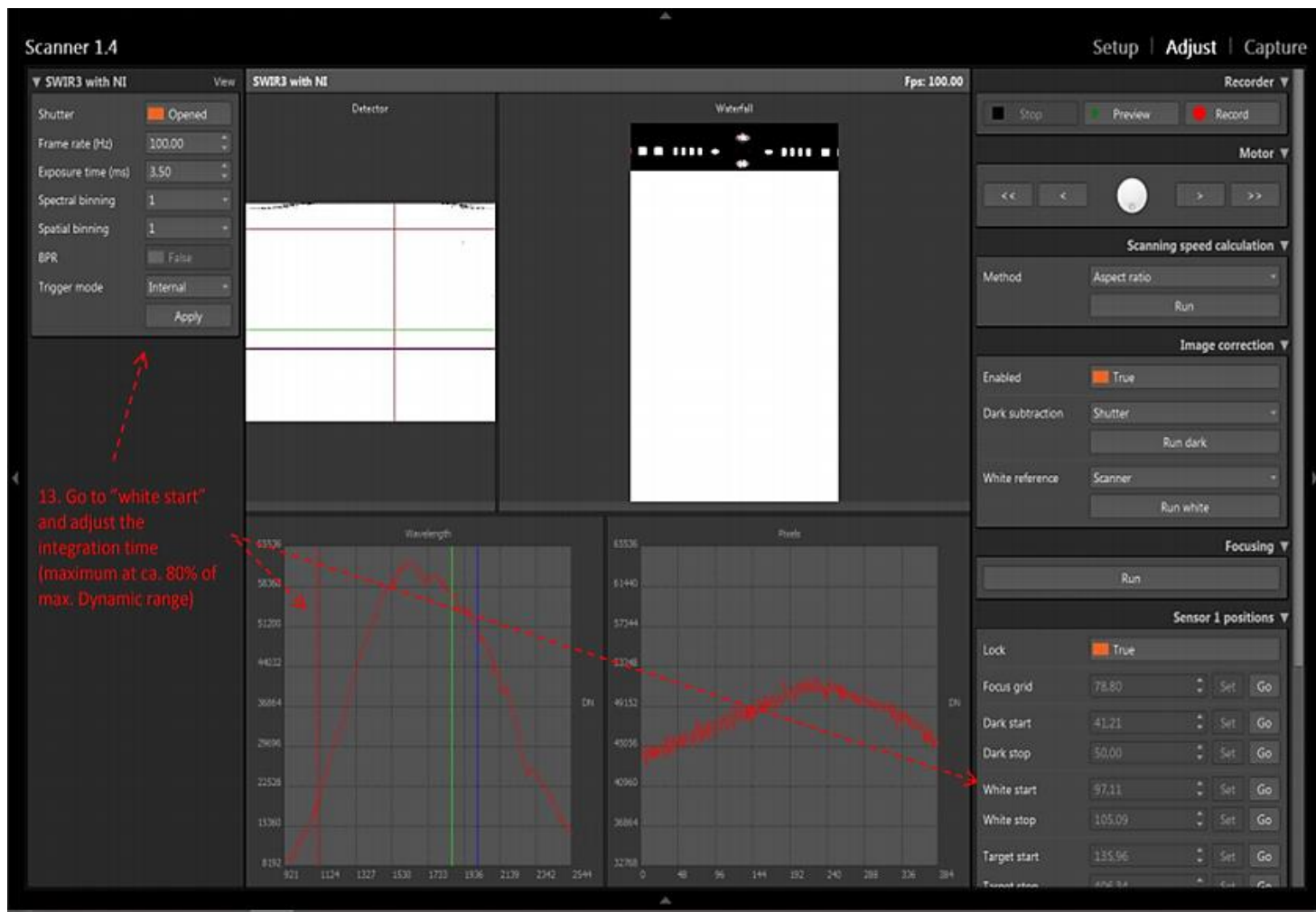


Figure 9: Prepare the Graph of Sample

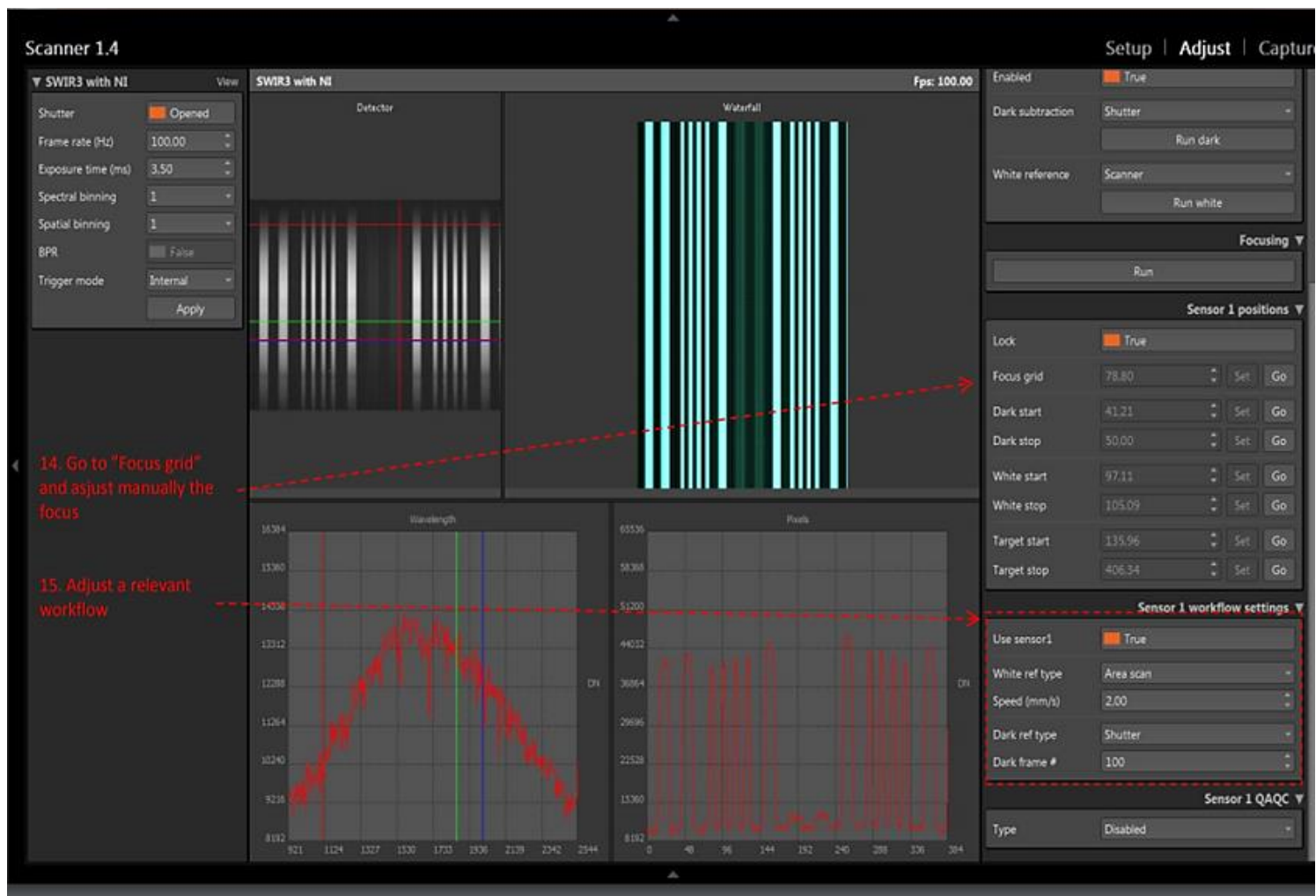


Figure 10: Adjusting of Workflow

### 3.3.6 Image Capture

The image capturing is as shown in the Figure 11, and it is done after adjusting the scanning speed. In order to save the image, firstly the preview option is to be used to view, and then using the record the image can be saved as shown in Figure 12.

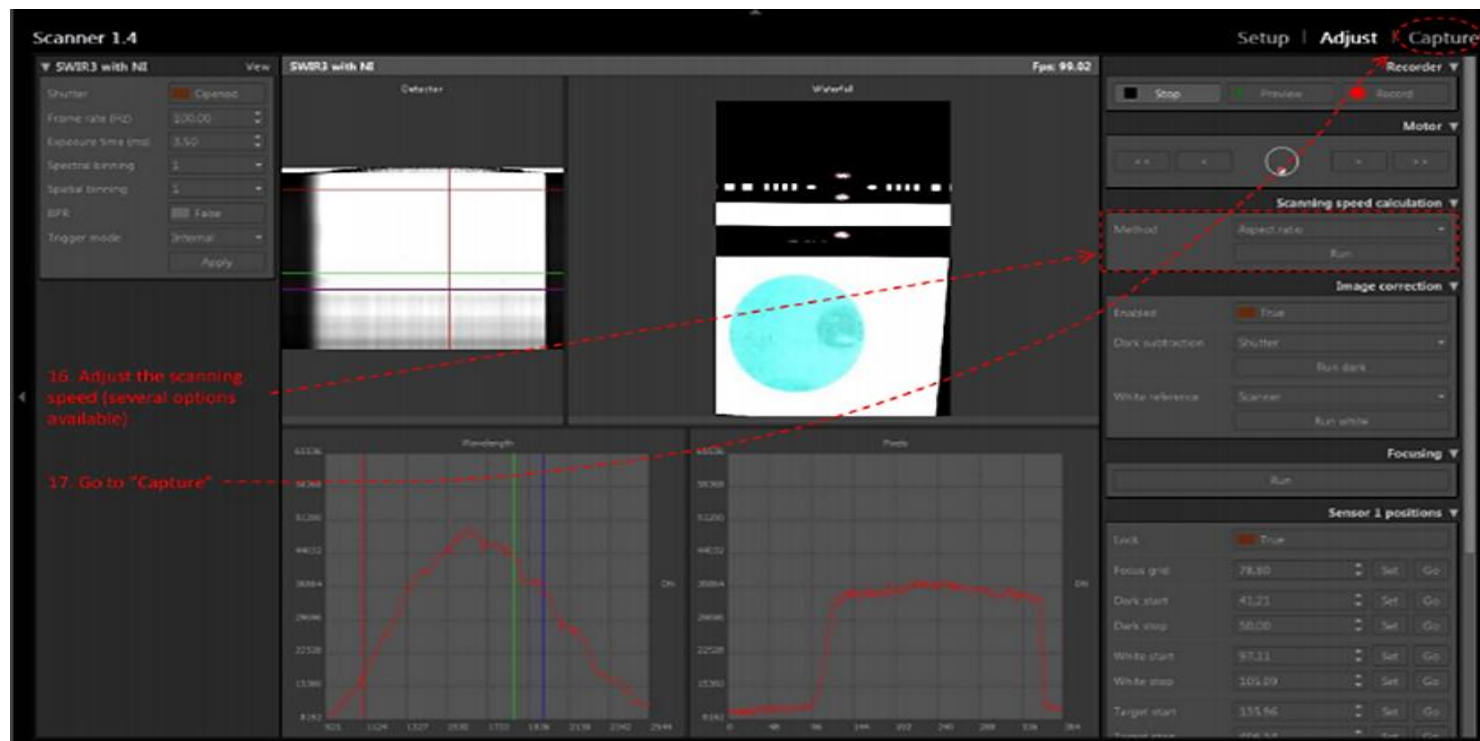


Figure 11: Image Capture

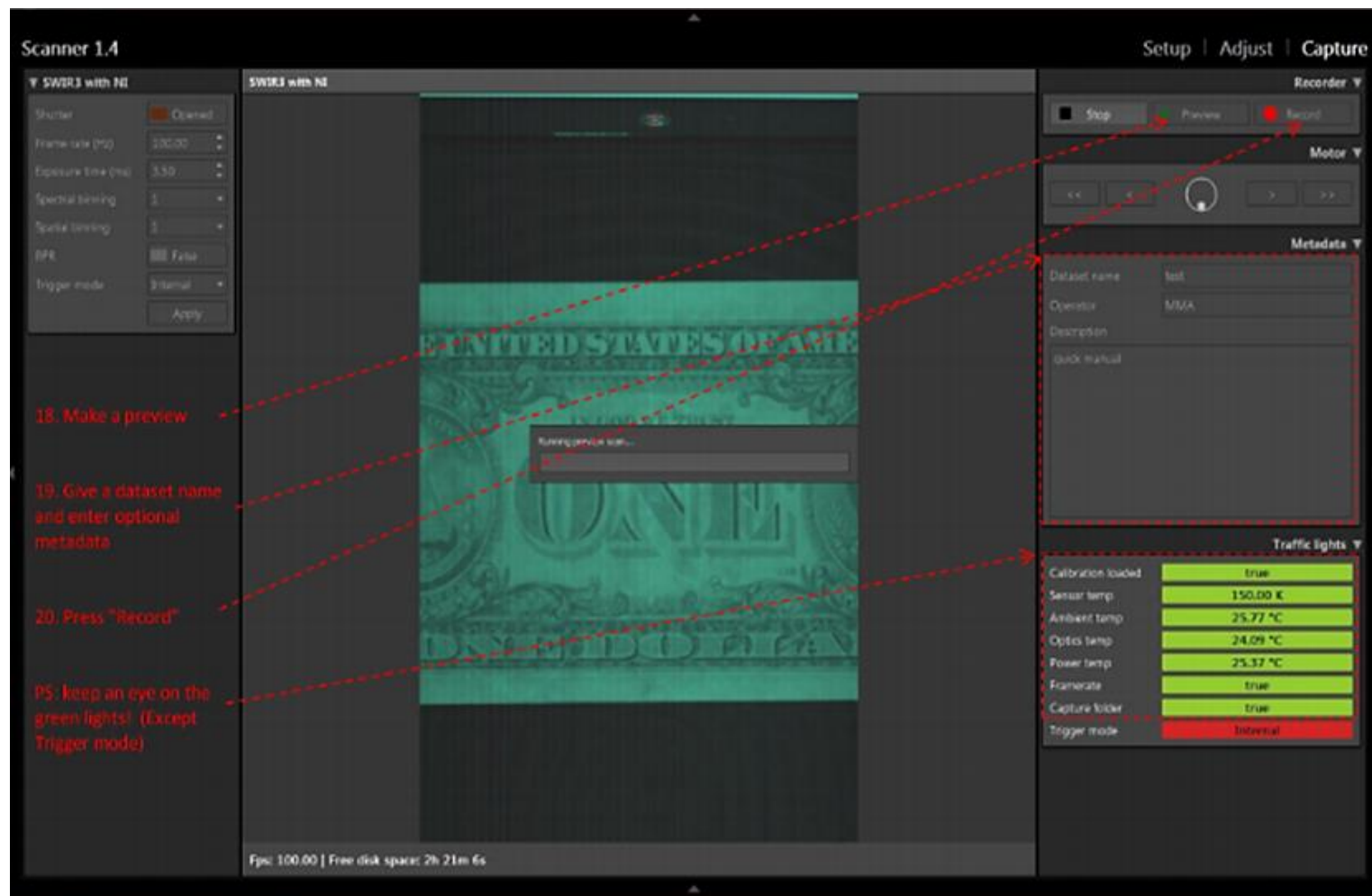


Figure 12: Save the Image

### 3.4 Analyzing Data

The outcomes of analyzing shows the graph for each sample of leaf. The graph shows the wavelength and the reflectance of leaf sample. Leaf Samples for each cultivar has different wavelength from other. The graphs have been created by camera software.

After processing the leaf photos and displaying the wavelength of each cultivar and the reflectance of light in wavelength, analyzed data by using Excel Program to create the graph for each cultivar between reflectance and wavelength. This step to see the range of wavelength of each cultivar.

Second step is calculated frequencies, cumulative proportion and cumulative percentages of each reflectance point for each cultivar by using Excel Program to see the highest and lowest frequency of each cultivar.

After that, using Excel Program to draw the graph which show curves for all cultivars for better comparison to see in which points the curves differ to each other and which point cross to others.

Then, calculated the sample variance and standard deviation by Excel Program to detect the critical point for comparison.

Finally, the Kolmogorov-Smirnov Normality Test (K-S Test) was performed in order to compare studied cultivars by using Excel program.

## Chapter 4: Results

After processing the leaf photos and displaying the wavelength of each cultivar and the reflectance of light in wavelength, analyzed data showed that, the range of wavelength of all cultivars are between 400 and 1000 and the range of reflectance is between 0.3 and 1 for Barhi, Khenezi, Khalas, Khadrawi, Fard, and Helali, as shown respectively in Figures 12-17.

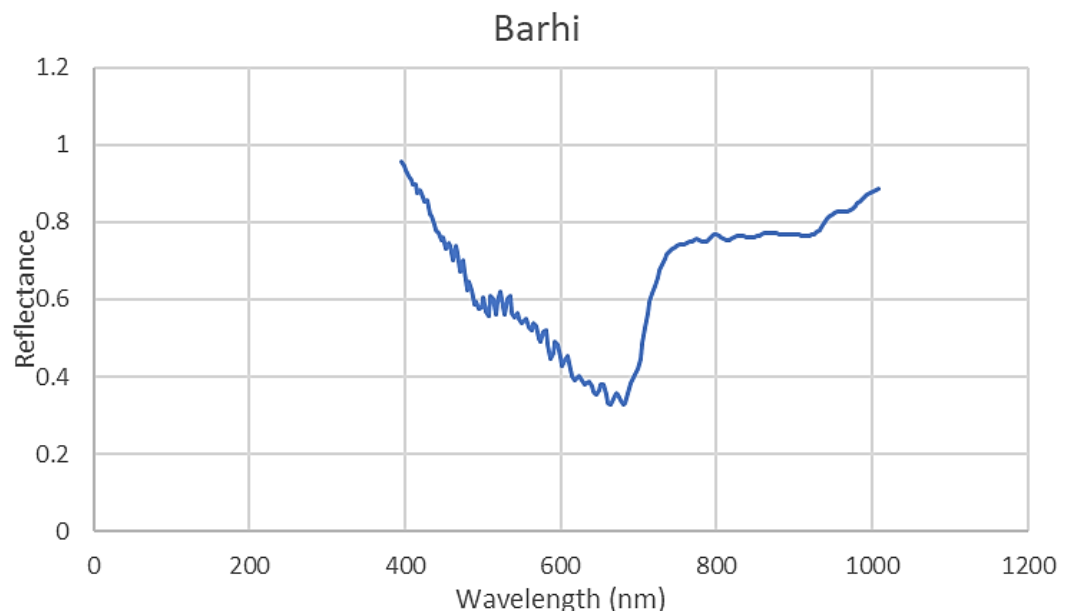


Figure 13: Reflectance versus Wavelength of Barhi

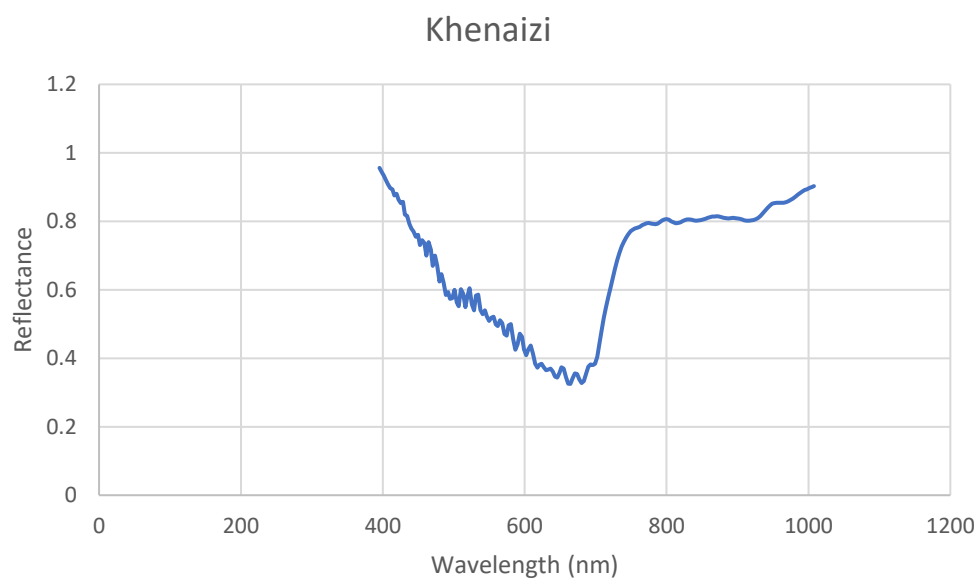


Figure 14: Reflectance versus Wavelength of Khenazi

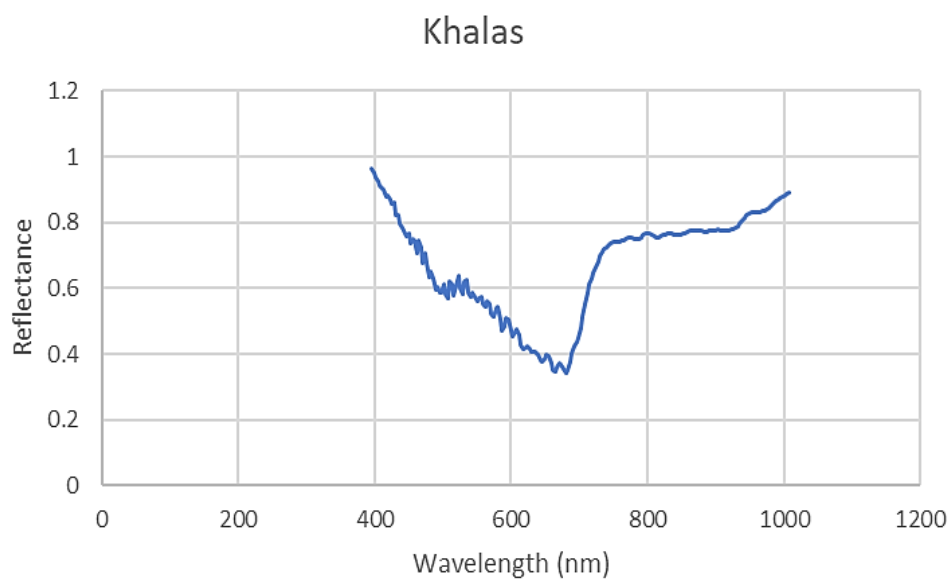


Figure 15: Reflectance versus Wavelength of Khalas

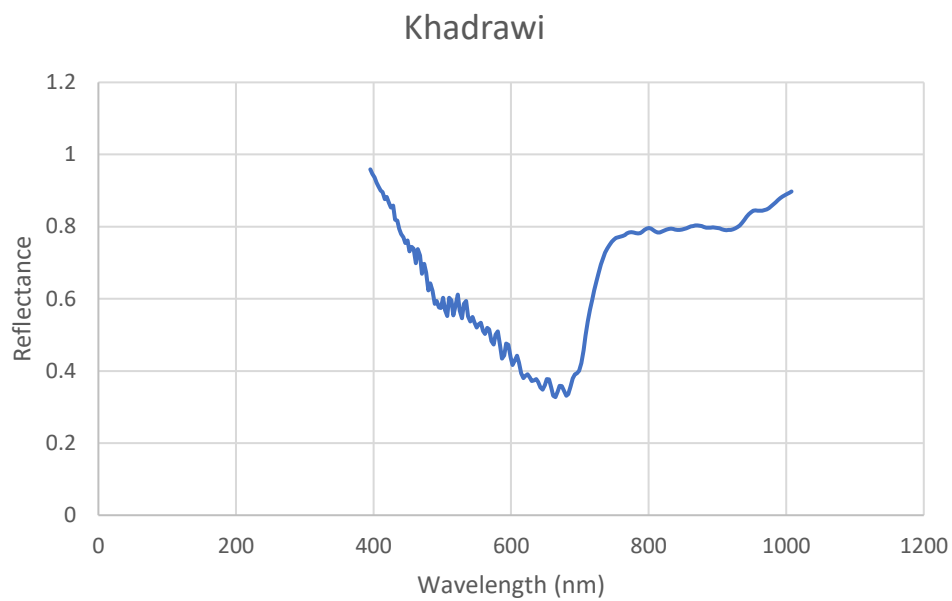


Figure 16: Reflectance versus Wavelength of Khadrawi

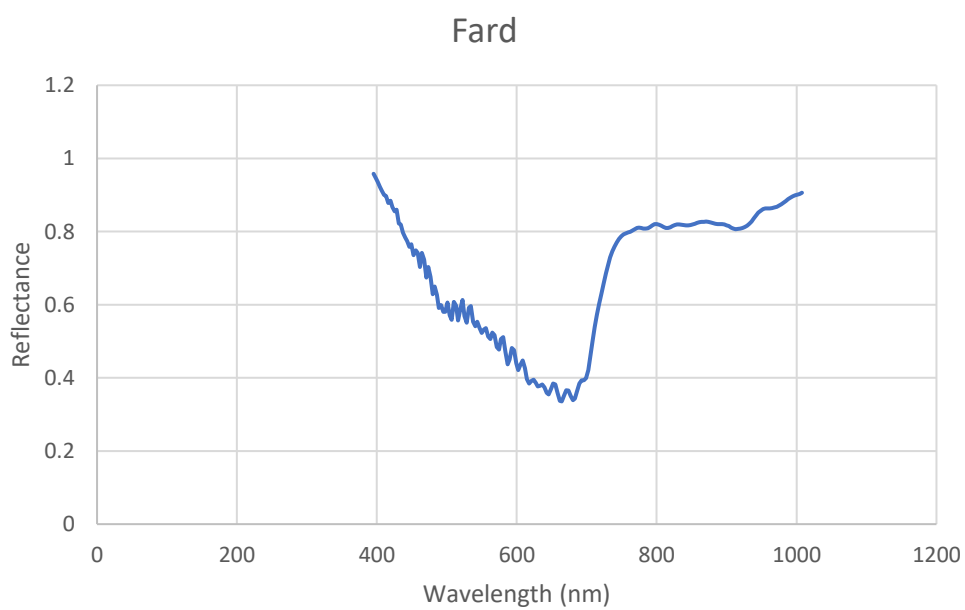


Figure 17: Reflectance versus Wavelength of Fard



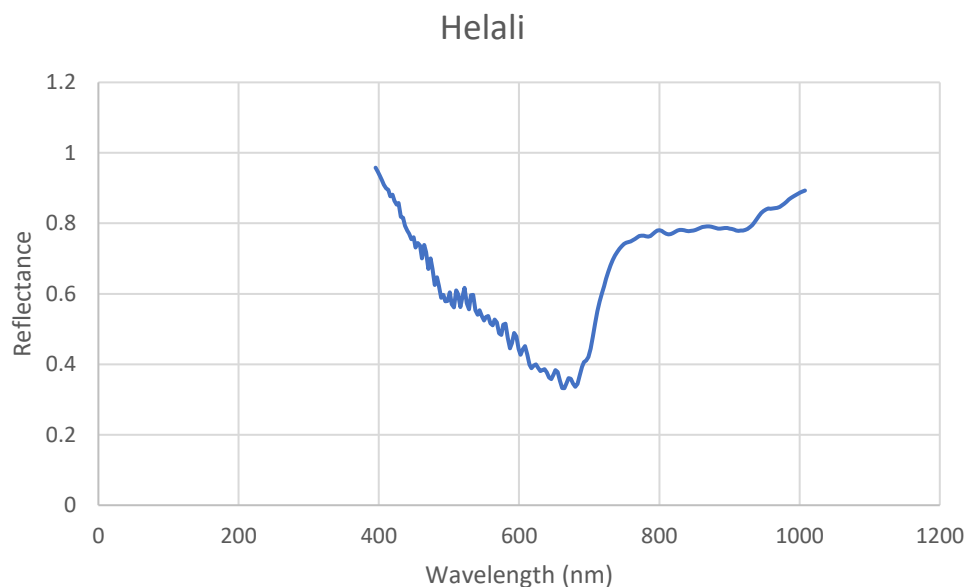


Figure 18: Reflectance versus Wavelength of Helali

On the other hand calculated frequencies, cumulative proportion and cumulative percentages of each reflectance point for each cultivar showed that, the highest frequency in Barhi cultivar is 49 in reflectance 0.822814, while the lowest frequency is 1 in reflectance 0.329974 (Figure 18), the highest frequency in Khenazi is 64 in reflectance 0.776956, while the lowest frequency is 1 in reflectance 0.327765 (Figure 19), the highest frequency in Khalas is 64 in reflectance 0.823069, while the lowest frequency is 1 in reflectance 0.330217 (Figure 20), the highest frequency in Khadrawi is 59 in reflectance 0.770903, while the lowest frequency is 1 in reflectance 0.310582 (Figure 21), the highest frequency in Fard is 50 in reflectance 0.830062, while the lowest frequency is 1 in reflectance 0.364221 (Figure 22), and the highest frequency in Helali is 64 in reflectance 0.824555, while the lowest frequency is 1 in reflectance 0.341369 (Figure 23).

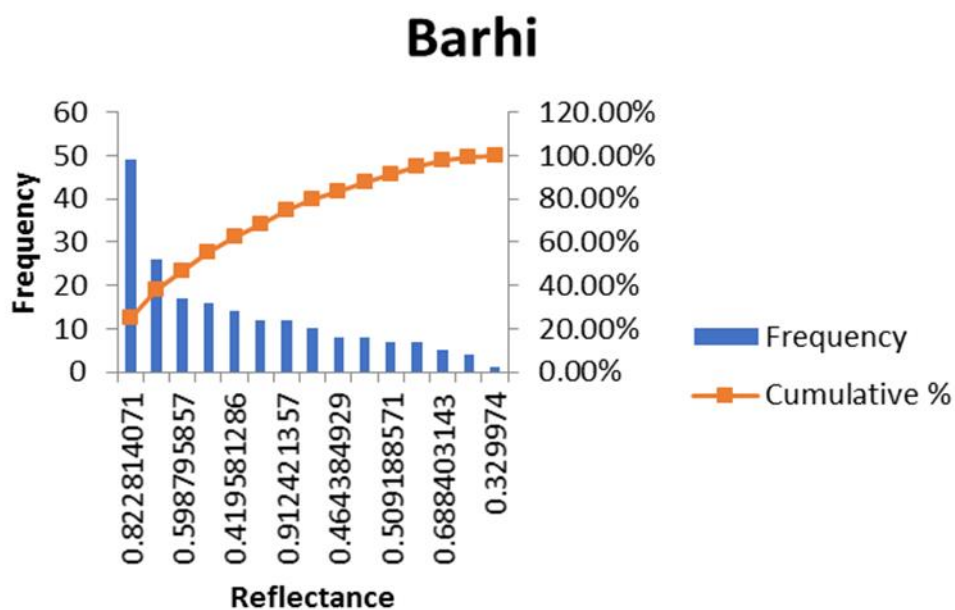


Figure 19: Reflectance versus Frequency of Barhi

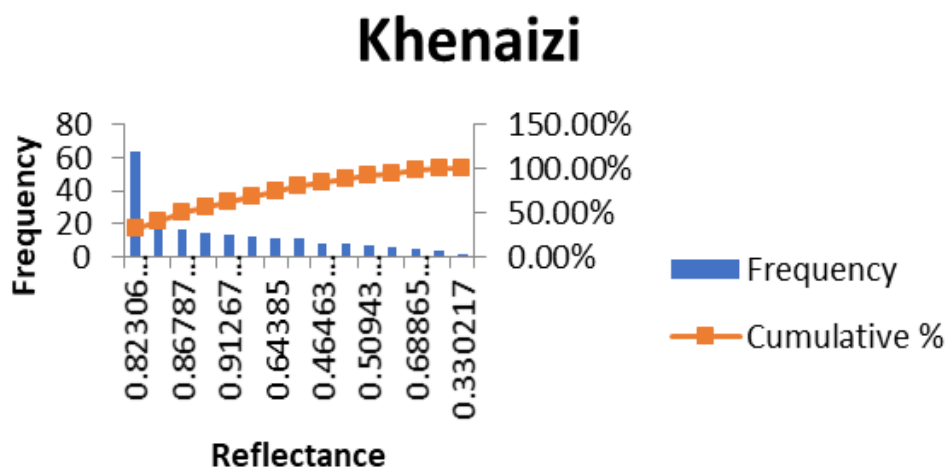


Figure 20: Reflectance versus Frequency of Khenaizi

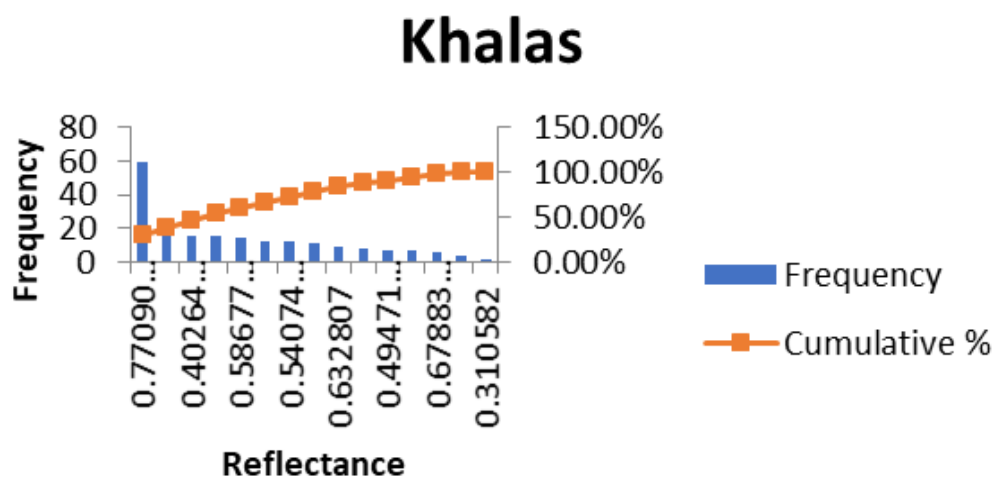


Figure 21: Reflectance versus Frequency of Khalas

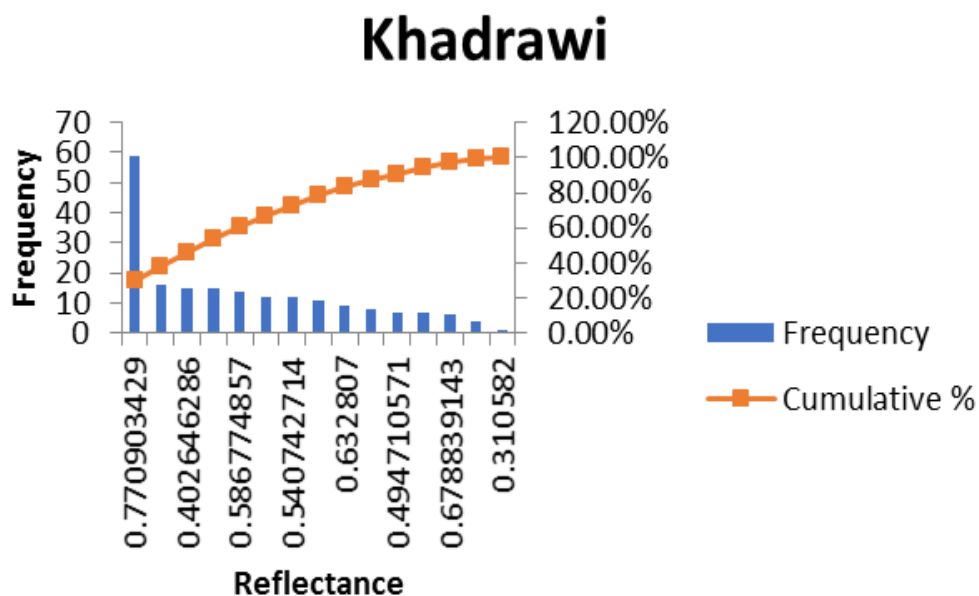


Figure 22: Reflectance versus Frequency of Khadrawi

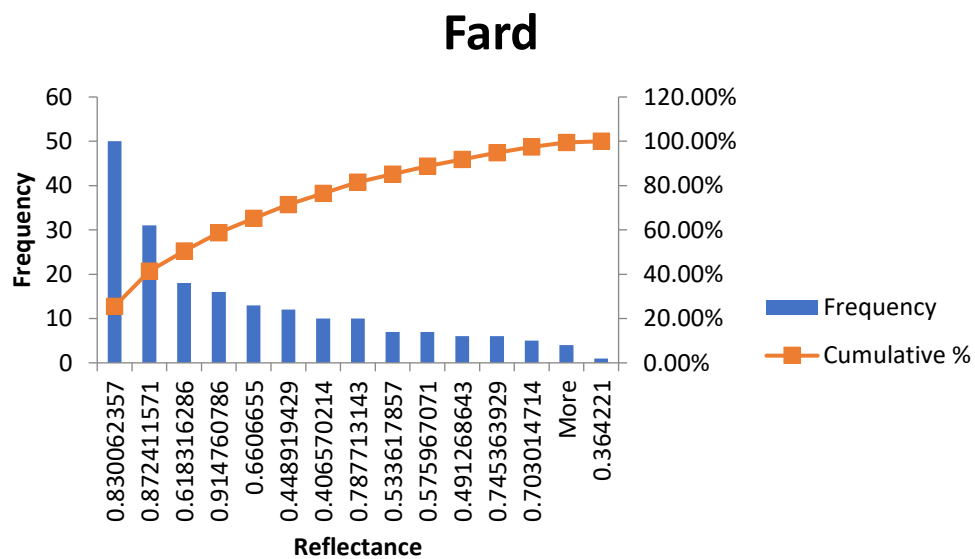


Figure 23: Reflectance versus Frequency of Fard

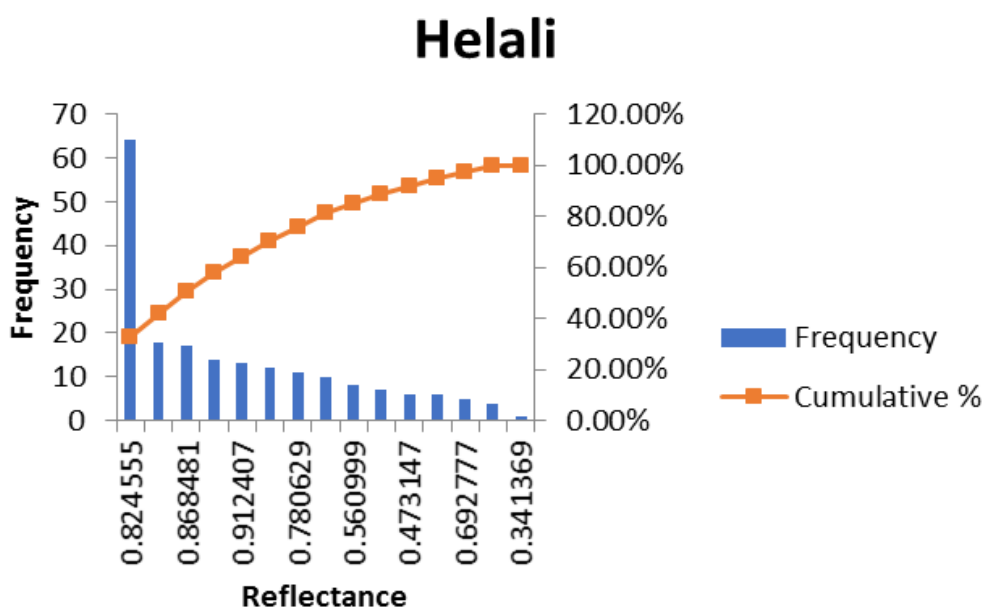


Figure 24: Reflectance versus Frequency of Helali



For better comparison drawing curves were displayed together, showed that, each cultivar has its unique figure, despite that for some wavelength intervals, some or all cultivars curves are crossed or even unified (Figure 24).

The numeric data of reflectance, frequencies, and cumulative percentages for all cultivars are shown in (Appendix 1).

Using the ranges of reflectance for each cultivar at each point of wavelength between 395.35-1007.71 nm, statistic readings basically standard deviation and sample variance were calculated, the highest standard deviation and sample variance marked at 705.25 nm point, (as shown in Figure 25 and Figure 26), suggesting that, this wavelength point could be the center of a promising distinguishing interval between the cultivars of study.

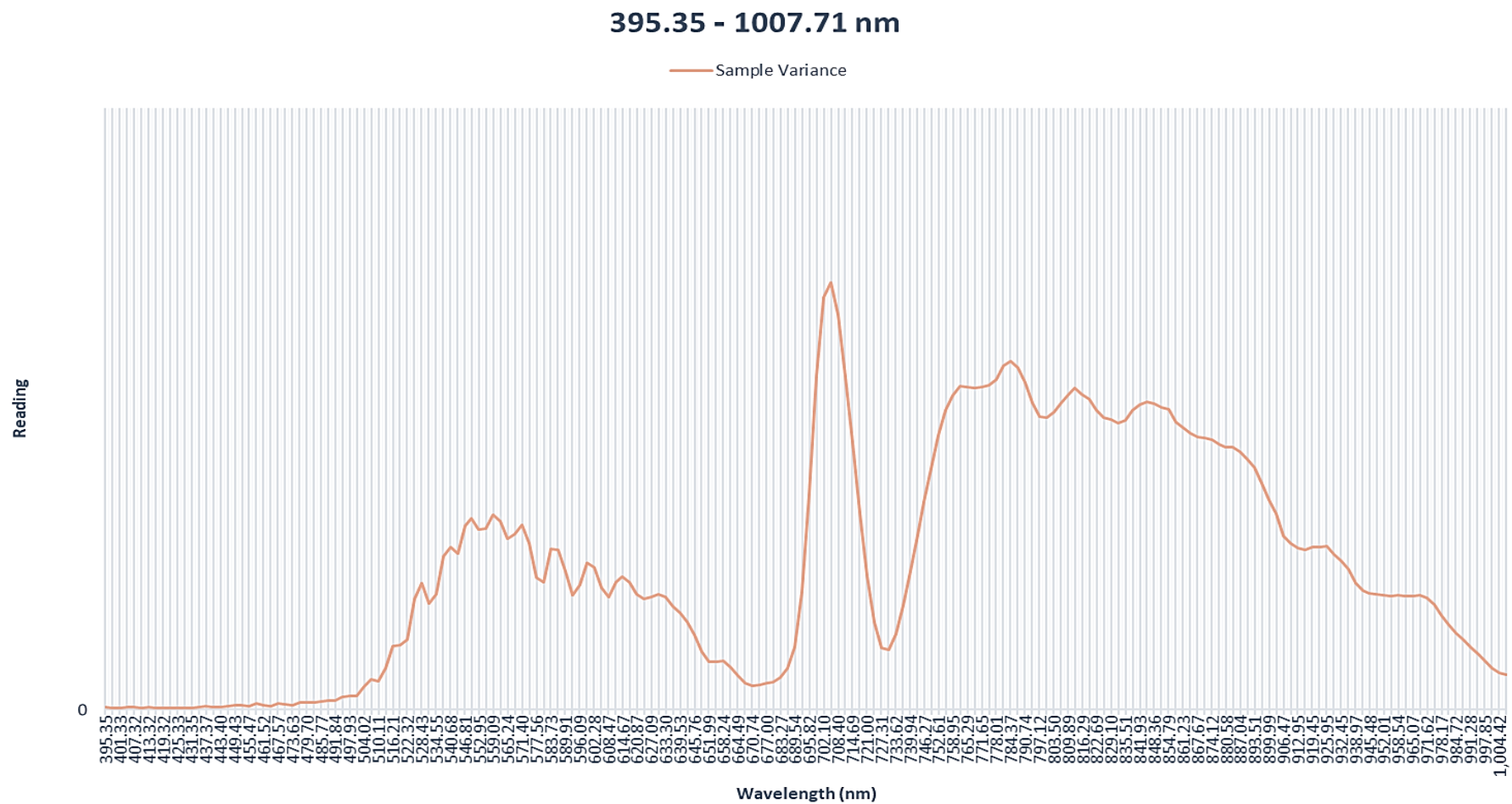


Figure 26: Sample Variance

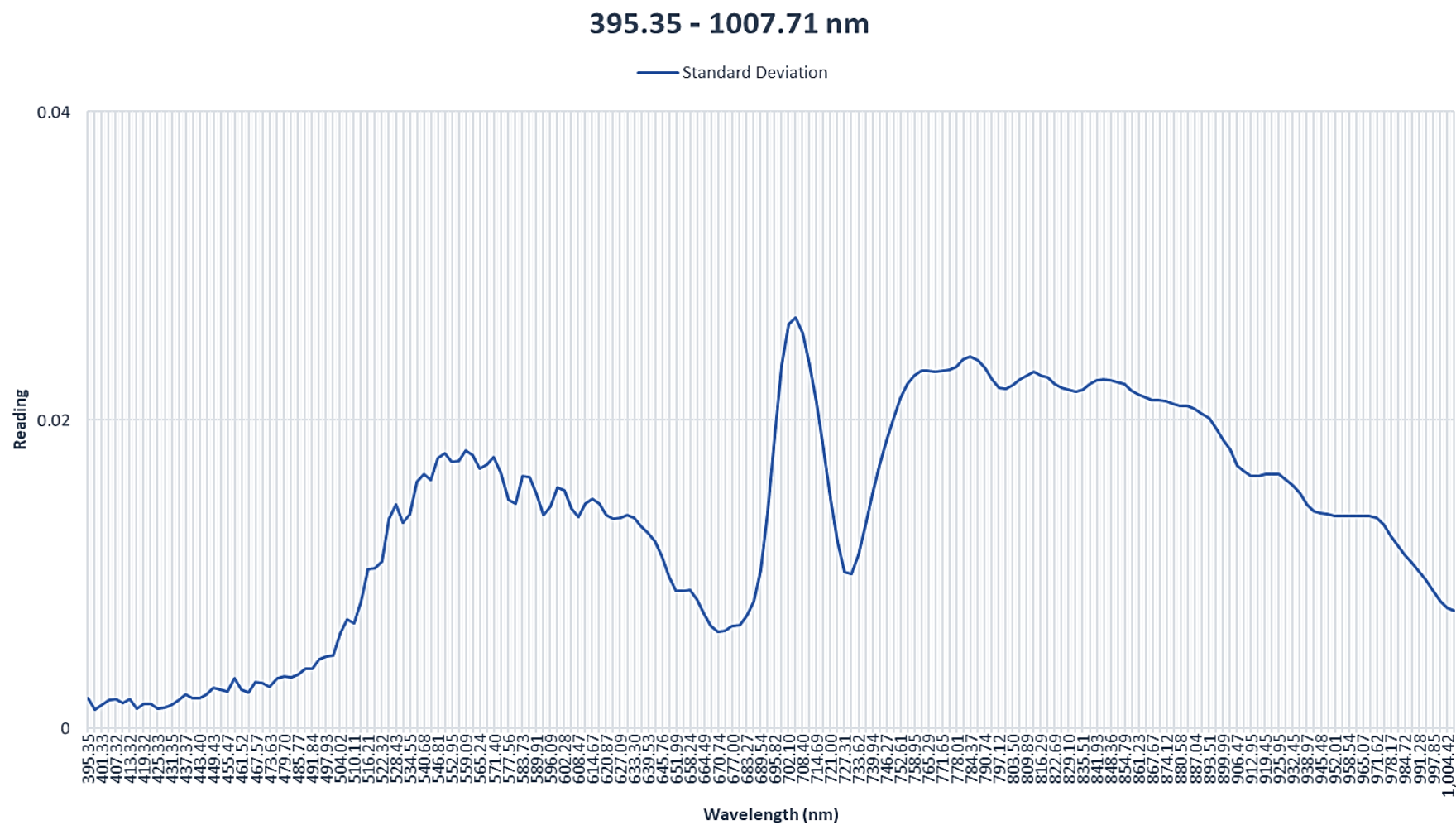


Figure 27: Standard Deviation



At 705.25 nm point, Khalas (0.514393), Barhi (0.485868), and Helali (0.478543) showed higher readings than others while Khenezi (0.4388) reflect the lowest (Figure 27), Khadrawi (0.457729), and Red Fard (0.457551) reflect the same result at this point while they showed clear differentiation at others (Figure 24). The numeric data of reflectance ranges, standard deviations and sample variances for all cultivars are shown in (Appendix 2).

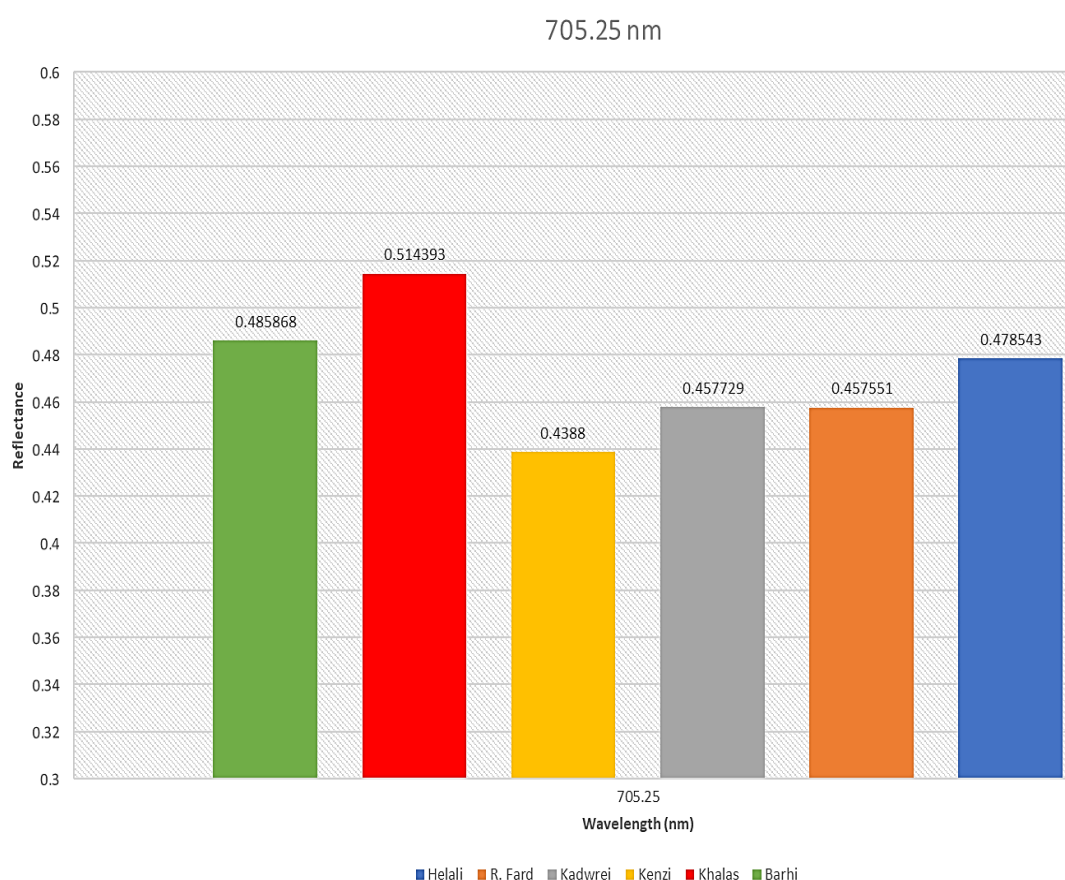


Figure 28: Reflectance at 705.25 nm

Further calculations were made to confirm the accuracy of this study in order to find the best wavelength interval to comparison all species, cumulative percentage is another way of expressing frequency distribution, to find the value the number of times the reflectance occurred was divided by the total sample size. The main advantage of cumulative percentage over cumulative frequency as a measure of frequency distribution, is that it provides an easier way to compare different sets of data, using the cumulative proportion data (Table 1 and 2), Kolmogorov-Smirnov Normality Test (K-S Test) was performed to compare studied cultivars as pairs, the finding obtained is true regarding comparing Khalas with only Khadrawi, Fard and Helali, while it can't be said that the same is achieved for the other pairs because the differentiation between maximum difference and critic maximum difference doesn't reach the expected number (Table 3). The K-S Test do confirm the study finding as shown in (Figure 27), that Khadrawi and Fard couldn't be distinguished at 705.25 nm, still results were promising and only show a humble, but very important base for future studies on more samples, different sites and applying sophisticated statistics in order to find scientific reliable algorithms.

Table 1: Cumulative Proportion of Reflectance for Barhi, Khenaizi, and Khalas

	Barhi			Khenaizi			Khalas		
Reflectance	Frequency	Proportion	Cum. Prop.	Frequency	Proportion	Cum. Prop.	Frequency	Proportion	Cum. Prop.
0.329974	1	0.002610966	0.002610966	1	0.002610966	0.002610966	1	0.002610966	0.002610966
0.374777643	12	0.031331593	0.033942559	12	0.031331593	0.033942559	12	0.031331593	0.033942559
0.419581286	14	0.036553525	0.070496084	14	0.036553525	0.070496084	15	0.039164491	0.07310705
0.464384929	8	0.020887728	0.091383812	8	0.020887728	0.091383812	8	0.020887728	0.093994778
0.509188571	7	0.018276762	0.109660574	7	0.018276762	0.109660574	7	0.018276762	0.11227154
0.553992214	8	0.020887728	0.130548303	8	0.020887728	0.130548303	12	0.031331593	0.143603133
0.598795857	17	0.044386423	0.174934726	16	0.041775457	0.17232376	14	0.036553525	0.180156658
0.6435995	10	0.026109661	0.201044386	11	0.028720627	0.201044386	9	0.023498695	0.203655352
0.688403143	5	0.01305483	0.214099217	5	0.01305483	0.214099217	6	0.015665796	0.219321149
0.733206786	7	0.018276762	0.232375979	6	0.015665796	0.229765013	7	0.018276762	0.237597911
0.778010429	26	0.067885117	0.300261097	11	0.028720627	0.25848564	59	0.154046997	0.391644909
0.822814071	49	0.127937337	0.428198433	64	0.167101828	0.425587467	15	0.039164491	0.430809399
0.867617714	16	0.041775457	0.46997389	16	0.041775457	0.467362924	16	0.041775457	0.472584856
0.912421357	12	0.031331593	0.501305483	13	0.033942559	0.501305483	11	0.028720627	0.501305483
0.822814071	49	0.127937337	0.62924282	64	0.167101828	0.668407311	59	0.154046997	0.65535248
0.778010429	26	0.067885117	0.697127937	16	0.041775457	0.710182768	16	0.041775457	0.697127937
0.598795857	17	0.044386423	0.74151436	16	0.041775457	0.751958225	15	0.039164491	0.736292428
0.867617714	16	0.041775457	0.783289817	14	0.036553525	0.788511749	15	0.039164491	0.775456919
0.419581286	14	0.036553525	0.819843342	13	0.033942559	0.822454308	14	0.036553525	0.812010444

Table 1: Cumulative Proportion of Reflectance for Barhi, Khenazi, and Khalas (continued)

	Barhi			Khenazi			Khalas		
0.374777643	12	0.031331593	0.851174935	12	0.031331593	0.853785901	12	0.031331593	0.843342037
0.912421357	12	0.031331593	0.882506527	11	0.028720627	0.882506527	12	0.031331593	0.874673629
0.6435995	10	0.026109661	0.908616188	11	0.028720627	0.911227154	11	0.028720627	0.903394256
0.464384929	8	0.020887728	0.929503916	8	0.020887728	0.932114883	9	0.023498695	0.92689295
0.553992214	8	0.020887728	0.950391645	8	0.020887728	0.953002611	8	0.020887728	0.947780679
0.509188571	7	0.018276762	0.968668407	7	0.018276762	0.971279373	7	0.018276762	0.966057441
0.733206786	7	0.018276762	0.98694517	6	0.015665796	0.98694517	7	0.018276762	0.984334204
0.688403143	5	0.01305483	1	5	0.01305483	1	6	0.015665796	1
	383.00			383.00			383.00		

Table 2: Cumulative Proportion of Reflectance for Khadwri, Fard and Helali

	Khadrawi			Fard			Helali		
Reflectance	Frequency	Proportion	Cum. Prop.	Frequency	Proportion	Cum. Prop.	Frequency	Proportion	Cum. Prop.
0.329974	1	0.002610966	0.002610966	1	0.002610966	0.002610966	1	0.002610966	0.002610966
0.374777643	10	0.026109661	0.028720627	10	0.026109661	0.028720627	12	0.031331593	0.033942559
0.419581286	12	0.031331593	0.060052219	12	0.031331593	0.060052219	14	0.036553525	0.070496084
0.464384929	6	0.015665796	0.075718016	6	0.015665796	0.075718016	6	0.015665796	0.08616188
0.509188571	7	0.018276762	0.093994778	7	0.018276762	0.093994778	7	0.018276762	0.104438642
0.553992214	7	0.018276762	0.11227154	7	0.018276762	0.11227154	8	0.020887728	0.125326371
0.598795857	18	0.046997389	0.15926893	18	0.046997389	0.15926893	18	0.046997389	0.17232376
0.6435995	13	0.033942559	0.193211488	13	0.033942559	0.193211488	10	0.026109661	0.19843342
0.688403143	5	0.01305483	0.206266319	5	0.01305483	0.206266319	5	0.01305483	0.211488251
0.733206786	6	0.015665796	0.221932115	6	0.015665796	0.221932115	6	0.015665796	0.227154047
0.778010429	10	0.026109661	0.248041775	10	0.026109661	0.248041775	11	0.028720627	0.255874674
0.822814071	50	0.130548303	0.378590078	50	0.130548303	0.378590078	64	0.167101828	0.422976501
0.867617714	31	0.080939948	0.459530026	31	0.080939948	0.459530026	17	0.044386423	0.467362924
0.912421357	16	0.041775457	0.501305483	16	0.041775457	0.501305483	13	0.033942559	0.501305483
0.822814071	50	0.130548303	0.631853786	50	0.130548303	0.631853786	64	0.167101828	0.668407311
0.778010429	31	0.080939948	0.712793734	31	0.080939948	0.712793734	18	0.046997389	0.7154047
0.598795857	18	0.046997389	0.759791123	18	0.046997389	0.759791123	17	0.044386423	0.759791123
0.867617714	16	0.041775457	0.80156658	16	0.041775457	0.80156658	14	0.036553525	0.796344648
0.419581286	13	0.033942559	0.835509138	13	0.033942559	0.835509138	13	0.033942559	0.830287206
0.374777643	12	0.031331593	0.866840731	12	0.031331593	0.866840731	12	0.031331593	0.861618799

Table 2: Cumulative Proportion of Reflectance for Khadwri, Fard and Helali (continued)

	Khadrawi			Fard			Helali		
0.912421357	10	0.026109661	0.892950392	10	0.026109661	0.892950392	11	0.028720627	0.890339426
0.6435995	10	0.026109661	0.919060052	10	0.026109661	0.919060052	10	0.026109661	0.916449086
0.464384929	7	0.018276762	0.937336815	7	0.018276762	0.937336815	8	0.020887728	0.937336815
0.553992214	7	0.018276762	0.955613577	7	0.018276762	0.955613577	7	0.018276762	0.955613577
0.509188571	6	0.015665796	0.971279373	6	0.015665796	0.971279373	6	0.015665796	0.971279373
0.733206786	6	0.015665796	0.98694517	6	0.015665796	0.98694517	6	0.015665796	0.98694517
0.688403143	5	0.01305483	1	5	0.01305483	1	5	0.01305483	1
	383.00			383.00			383.00		

Table 3: Kolmogorov-Smirnov Normality Test (K-S Test)

	Barhi					Kenzi				Khalas			Khadwri		R F
	barhi&kenzi	barhi&khalas	barhi&khadwri	barhi&R F	barhi&helali	kenzi&khalas	kenzi&khadwri	kenzi&R F	kenzi&helali	khalas&khadwri	khalas&R F	khalas&helali	khadwri&R F	khadwri&helali	R F&helali
	0.0000000	0.0000000	0.0000000	0.0000000	0.0000000	0.0000000	0.0000000	0.0000000	0.0000000	0.0000000	0.0000000	0.0000000	0.0000000	0.0000000	0.0000000
	0.0000000	0.0000000	0.00522193	0.00522193	0.0000000	0.0000000	0.00522193	0.00522193	0.0000000	0.00522193	0.00522193	0.0000000	0.0000000	-0.00522193	-0.00522193
	0.0000000	-0.00261097	0.01044386	0.01044386	0.0000000	-0.00261097	0.01044386	0.01044386	0.0000000	0.01305483	0.01305483	0.00261097	0.0000000	-0.01044386	-0.01044386
	0.0000000	-0.00261097	0.01566580	0.01566580	0.00522193	-0.00261097	0.01566580	0.01566580	0.00522193	0.01827676	0.01827676	0.00783290	0.0000000	-0.01044386	-0.01044386
	0.0000000	-0.00261097	0.01566580	0.01566580	0.00522193	-0.00261097	0.01566580	0.01566580	0.00522193	0.01827676	0.01827676	0.00783290	0.0000000	-0.01044386	-0.01044386
	0.0000000	-0.01305483	0.01827676	0.01827676	0.00522193	-0.01305483	0.01827676	0.01827676	0.00522193	0.03133159	0.03133159	0.01827676	0.0000000	-0.01305483	-0.01305483
	0.00261097	-0.00522193	0.01566580	0.01566580	0.00261097	-0.00783290	0.01305483	0.01305483	0.0000000	0.02088773	0.02088773	0.00783290	0.0000000	-0.01305483	-0.01305483
	0.0000000	-0.00261097	0.00783290	0.00783290	0.00261097	-0.00261097	0.00783290	0.00783290	0.00261097	0.01044386	0.01044386	0.00522193	0.0000000	-0.00522193	-0.00522193
	0.0000000	-0.00522193	0.00783290	0.00783290	0.00261097	-0.00522193	0.00783290	0.00783290	0.00261097	0.01305483	0.01305483	0.00783290	0.0000000	-0.00522193	-0.00522193
	0.00261097	-0.00522193	0.01044386	0.01044386	0.00522193	-0.00783290	0.00783290	0.00783290	0.00261097	0.01566580	0.01566580	0.01044386	0.0000000	-0.00522193	-0.00522193
	0.04177546	-0.09138381	0.05221932	0.05221932	0.04438642	-0.13315927	0.01044386	0.01044386	0.00261097	0.14360313	0.14360313	0.13577023	0.0000000	-0.00783290	-0.00783290
	0.00261097	-0.00261097	0.04960836	0.04960836	0.00522193	-0.00522193	0.04699739	0.04699739	0.00261097	0.05221932	0.05221932	0.00783290	0.0000000	-0.04438642	-0.04438642
	0.00261097	-0.00261097	0.01044386	0.01044386	0.00261097	-0.00522193	0.00783290	0.00783290	0.0000000	0.01305483	0.01305483	0.00522193	0.0000000	-0.00783290	-0.00783290
	0.0000000	0.0000000	0.0000000	0.0000000	0.0000000	0.0000000	0.0000000	0.0000000	0.0000000	0.0000000	0.0000000	0.0000000	0.0000000	0.0000000	0.0000000
	-0.03916449	-0.02610966	-0.00261097	-0.00261097	-0.03916449	0.01305483	0.03655352	0.03655352	0.0000000	0.02349869	0.02349869	-0.01305483	0.0000000	-0.03655352	-0.03655352
	-0.01305483	0.0000000	-0.01566580	-0.01566580	-0.01827676	0.01305483	-0.00261097	-0.00261097	-0.00522193	-0.01566580	-0.01566580	-0.01827676	0.0000000	-0.00261097	-0.00261097
	-0.01044386	0.00522193	-0.01827676	-0.01827676	-0.01827676	0.01566580	-0.00783290	-0.00783290	-0.00783290	-0.02349869	-0.02349869	-0.02349869	0.0000000	0.0000000	0.0000000
	-0.00522193	0.00783290	-0.01827676	-0.01827676	-0.01305483	0.01305483	-0.01305483	-0.01305483	-0.00783290	-0.02610966	-0.02610966	-0.02088773	0.0000000	0.00522193	0.00522193
	-0.00261097	0.00783290	-0.01566580	-0.01566580	-0.01044386	0.01044386	-0.01305483	-0.01305483	-0.00783290	-0.02349869	-0.02349869	-0.01827676	0.0000000	0.00522193	0.00522193
	-0.00261097	0.00783290	-0.01566580	-0.01566580	-0.01044386	0.01044386	-0.01305483	-0.01305483	-0.00783290	-0.02349869	-0.02349869	-0.01827676	0.0000000	0.00522193	0.00522193
	0.0000000	0.00783290	-0.01044386	-0.01044386	-0.00783290	0.00783290	-0.01044386	-0.01044386	-0.00783290	-0.01827676	-0.01827676	-0.01566580	0.0000000	0.00261097	0.00261097
	-0.00261097	0.00522193	-0.01044386	-0.01044386	-0.00783290	0.00783290	-0.00783290	-0.00783290	-0.00522193	-0.01566580	-0.01566580	-0.01305483	0.0000000	0.00261097	0.00261097
	-0.00261097	0.00261097	-0.00783290	-0.00783290	-0.00783290	0.00522193	-0.00522193	-0.00522193	-0.00522193	-0.01044386	-0.01044386	-0.01044386	0.0000000	0.0000000	0.0000000
	-0.00261097	0.00261097	-0.00522193	-0.00522193	-0.00522193	0.00522193	-0.00261097	-0.00261097	-0.00261097	-0.00783290	-0.00783290	-0.00783290	0.0000000	0.0000000	0.0000000
	-0.00261097	0.00261097	-0.00261097	-0.00261097	-0.00261097	0.00522193	0.0000000	0.0000000	0.0000000	-0.00522193	-0.00522193	-0.00522193	0.0000000	0.0000000	0.0000000
	0.0000000	0.00261097	0.0000000	0.0000000	0.0000000	0.00261097	0.0000000	0.0000000	0.0000000	-0.00261097	-0.00261097	-0.00261097	0.0000000	0.0000000	0.0000000
	0.0000000	0.0000000	0.0000000	0.0000000	0.0000000	0.0000000	0.0000000	0.0000000	0.0000000	0.0000000	0.0000000	0.0000000	0.0000000	0.0000000	0.0000000
Max. difference	0.04177546	0.00783290	0.05221932	0.05221932	0.04438642	0.01566580	0.04699739	0.04699739	0.00522193	0.14360313	0.14360313	0.13577023	0.0000000	0.00522193	0.00522193
critic Max. diff.	0.069492754	0.069492754	0.069492754	0.069492754	0.069492754	0.069492754	0.069492754	0.069492754	0.069492754	0.069492754	0.069492754	0.069492754	0.069492754	0.069492754	0.069492754
difference	-0.02771730	-0.06165986	-0.01727343	-0.01727343	-0.02510633	-0.05382696	-0.02249536	-0.02249536	-0.06427082	0.07411038	0.07411038	0.06627748	-0.06949275	-0.06427082	-0.06427082

## Chapter 5: Discussion

The six tested cultivars of date palms which are Barhi, Khadrawi, Khenazi, Khalas, Fard and Helali reported the 705.25 nm point as the highest in variance (Figure 14) and standard deviation (Figure 15) among the all tested wavelengths from 395.35 to 1007.71 nm (Appendix 1). Applied variance and standard deviation readings to see how numbers relate to each other within a data set, at this point (Figure 16) Khalas, Barhi, and Helali showing higher readings than others while Khenazi reflect the lowest. Khadrawi, and Fard reflect the same result at this point while they showed clear differentiation at others (Figure 13), so further study with more samples needed in order to find the best wavelength for comparison of all species.

On the other hand, by performing Kolmogorov-Smirnov Normality Test (K-S Test), using the cumulative proportion data (Table 1 and 2), comparing the six cultivars as pairs, it can be concluded statistically that previous finding is significant regarding comparison of Khalas with only Khadrawi, Fard and Helali, while this could not confirm the same for the other pairs because the differentiation between maximum difference and critic Maximum difference were in minus (Table 3).

The interpretation of hyperspectral images is accompanied by several different aspects, some related to the sensor technology compared to multispectral images or RGB images, other are related to an investigated phenomenon and the possibility to characterize, quantize and parametrize changes in the observations.

In this study, the RGB images data is used to find hyperspectral signature for samples (showing no visible changes to the naked eye), taken from healthy plants to eliminate any effect of problems related to diseases as, bacterial or fungal infections



and /or drought. So, in this study, the data is dealt without any standard or previous research results to directly compare with.

Previous studies using Hyperspectral technology imaging spectrometry technology and consider as one of the important leading research fields of remote sensing. Also, Hyperspectral remote sensing technology has been successfully applied in many fields as Jiang et al. (2004) described that Hyperspectral technology imaging spectrometry technology, is one of the important leading research fields of remote sensing. Since the first imaging spectrometer was produced in 1983, in less than 20 years. Hyperspectral remote sensing technology has been successfully applied in many fields and shown great potential and bright prospects. Research on processing, analysis and information extraction of Hyperspectral data should be strengthened to determine more useful information, make full use of the advantage and potential of Hyperspectral remote sensing technology, and promote the development of new and important technology (Jiang et al., 2004). Also, the results shows that this technique is useful and important in agriculture field. By this technique, the study outcomes are having noticed a difference between the leaves of date palms. Through this study, it is noticed that using this technique will save us too much time waiting the date fruits to ripe, need only few leaves to work on, and cost nothing once the camera is ready and determining and the examining wavelength. The best Hyperspectral wavebands in the study of date palms and agricultural crops over the spectral range of 400 – 2500 nm and assessed the date palms and agricultural crop classification accuracies achievable using the various combinations of the best Hyperspectral narrow wavebands (Thenkabail et al., 2004). In this result, after processing the leaf photos, and displaying the wavelength of each cultivar and the reflectance of light in wavelength, analyzed data showed that, the range of wavelength of all cultivars are between 400 nm and 1000 nm. The spectral

range that Thenkabail et al. (2004) used is wider than the range considered in this study due to camera range, higher wavelengths until 2500 are recommended to be added to the camera machine to continue with this study and other colleges researchers.

The leaves of plants can trait the amount of light reflected from leaves. The work carried out by Esau et al. (2006) showed that the leaf traits and physiological performance govern the amount of light reflected from leaves at visible and infrared wavebands. Information on leaf optical properties of tropical trees is scarce. In this study the leaves of date palm trees and the darkness of leaves also could affect by the amount of light reflectance. It visualized that the difference in amount of reflectance from leaf to leaf is dependent on the amount of darkness of leaves which is the percentage of chlorophyll in leaves. However, depending on Esau result (2006), it was decided to work on control samples trying to delete any other factors that would affect the findings of this study. The concern noticed at this time was to distinguish the date types only with chlorophyll content.

According to the results obtained in this research, it is found that the results of Tarabalka (2011) is in agreement that large number of spectral bands acquired by Hyperspectral sensors increased the capability to distinguish physical materials and objects, and the proposed method improves classification accuracies when compared to other classification approaches. Future studies on palm trees need to link the hyperspectral metrics with other data that is generated from laboratory results on chlorophyll concentration, enzyme content, and/or any other biochemical parameters.

Sandmeier et al. (1998) reported a new approach for deriving vegetation canopy structural characteristics from Hyperspectral bi-directional reflectance distribution function (BRDF) data. The methodology is based on the relationship between spectral variability of BRDF effects and canopy geometry.

However, in this research using Hyperspectral Camera to distinguish between the leaves of palm trees. The methodology is based on the relationship between wavelength and reflectance.

According to this study the result were similar to Rajabi and Ghassemian (2015) who studied a variety of feature reduction methods that have been developed by using spectral and spatial domains. In these studies, a feature extracting technique was proposed based on rational function curve fitting. For each pixel of a Hyperspectral image, a specific rational function approximation was developed to fit the spectral response curve of that pixel. Coefficients of the numerator and denominator polynomials of these functions were considered as new extracted features.

Teena et al. (2013) studied that the early stages of microbial infection in date palm fruits are difficult to detect by the presently used manual sorting technique. The potential of Hyperspectral imaging technique to detect fungal contamination of edible date fruits was investigated in their study. The samples were treated as three groups: Untreated Control (UC), Sterile Control (SC) (surface sterilized, rinsed and dried) and inoculated samples (IS) (surface sterilized, rinsed, dried and inoculated). While in this research, it was observed that there were very difficult to detect and classify the cultivars of date palm leaves in open fields because they were affected by many factors. So that, the samples were treated as under control (in tissue culture) to avoid any factors that could affect. This study is showing promising analysis of hyperspectral signature of various date palm leaves, the findings are starting point to contribute to a better detection of leaves optical properties for each type. This technology being so promising, further analytical methods and sensor specificities should be further studied for development of precise high throughput screening systems of differentiation.

## Chapter 6: Conclusions and Recommendations

The study investigated the effect of reflectance of light and frequency of each cultivar. Based on this study, it appears that some cultivar of date palm tree has different spectral signature with which can be precisely differentiate between date palm cultivars by applying this technology on date palm leaf.

In fact, results of this study also showed highest frequency of light reflected of each cultivar in Khalas, Helali and Khenazi cultivars. While the highest reflectance in Khalas and Fard Cultivar.

The six tested cultivars of date palm trees which are Barhi, Khadrawi, Khenazi, Khalas, RedFard and Helali report the 705.25 nm point as the highest in variance and standard deviation but, further study with more samples needed in order to find the best wavelength to comparison all species. On the other hand, utilizing K-S Test result, statistical comparison could be possible between Khalas Khadrawi, RedFard and Helali while, there was no significance with other cultivars.

Finally, this research was conducted with the purpose to provide an effective of Hyperspectral Technology for classification the date palm cultivars.

The following recommendations are provided from this study:

1. Investigate the variation in a species' leaf reflectance across different sites along the four seasons (multitemporal data).
2. Apply the study on open field samples.
3. Compare the results of this study with results considering taking and using remote airborne or satellite-borne sensors.
4. Classifications using individual and all four spectral bands (blue, green, red, and infrared; multispectral data).

## References

- Al-Dosary, N. M. N., Al-Dobai, S., & Faleiro, J. R. (2016). Review on the management of red palm weevil *Rhynchophorus ferrugineus* olivier in date palm *Phoenix dactylifera* L. *Emirates Journal of Food and Agriculture*, 28(1), 34–44.
- Arias, E., Hodder, A. J., & Oihabi, A. (2016). FAO support to date palm development around the world: 70 years of activity. *Emirates Journal of Food and Agriculture*, 28(1), 1–11.
- Blackburn, G. A. (2007). Hyperspectral remote sensing of plant pigments. *Journal of Experimental Botany*, 58(4), 855–867. <https://doi.org/10.1093/jxb/erl123>
- Büttner, A., & Röser, H. P. (2014). Hyperspectral remote sensing with the UAS “Stuttgarter Adler” - System setup, calibration and first results. *Photogrammetrie, Fernerkundung, Geoinformation*, 2014(4), 265–274.
- Chao, C. C. T., & Krueger, R. R. (2007). The date palm (*Phoenix dactylifera* L.): Overview of biology, uses, and cultivation. *HortScience*, 42(5), 1077–1082.
- Clevers, J. G. P. W., & Kooistra, L. (2012). Using hyperspectral remote sensing data for retrieving canopy chlorophyll and nitrogen content. *IEEE Journal of Selected Topics in Applied Earth Observations and Remote Sensing*, 5(2), 574–583.
- Esau, C., Davis, S., Murray, S. F., Yu, X. X., Pandey, S. K., Pear, M., Watts, L., Booten, S. L., Graham, M., McKay, R., Subramaniam, A., Propp, S., Lollo, B. A., Freier, S., Bennett, C. F., Bhanot, S., & Monia, B. P. (2006). miR-122 regulation of lipid metabolism revealed by in vivo antisense targeting. *Cell Metabolism*, 3(2), 87–98.
- Foody, G. M., Mathur, A., Sanchez-Hernandez, C., & Boyd, D. S. (2006). Training set size requirements for the classification of a specific class. *Remote Sensing of Environment*, 104(1), 1–14.
- Govender, N., Trollope, W. S. W., & Van Wilgen, B. W. (2006). The effect of fire season, fire frequency, rainfall and management on fire intensity in savanna vegetation in South Africa. *Journal of Applied Ecology*, 43(4), 748–758.
- Gros-Balthazard, M., Newton, C., Ivorra, S., Pintaud, J.-C., & Terral, J.-F. (2013). Origines et domestication du palmier dattier (*Phoenix dactylifera* L.): État de l’art et perspectives d’étude. *Revue d’ethnoécologie*, 4, 0–15.
- Hirano, A., Madden, M., & Welch, R. (2003). Hyperspectral image data for mapping wetland vegetation. *Wetlands*, 23(2), 436–448. <https://doi.org/10.1672/18-20>.

- Honkavaara, E., Saari, H., Kaivosoja, J., Pölönen, I., Hakala, T., Litkey, P., Mäkynen, J., & Pesonen, L. (2013). Processing and assessment of spectrometric, stereoscopic imagery collected using a lightweight UAV spectral camera for precision agriculture. *Remote Sensing*, 5(10), 5006–5039.
- Hruska, R., Mitchell, J., Anderson, M., & Glenn, N. F. (2012). Radiometric and geometric analysis of hyperspectral imagery acquired from an unmanned aerial vehicle. *Remote Sensing*, 4(9), 2736–2752. <https://doi.org/10.3390/rs4092736>
- Huang, L., Zhao, J., Chen, Q., & Zhang, Y. (2013). Rapid detection of total viable count (TVC) in pork meat by hyperspectral imaging. *Food Research International*, 54(1), 821–828.
- Jiang, Y., Yung, Y. L., Sander, S. P., & Travis, L. D. (2004). Modeling of atmospheric radiative transfer with polarization and its application to the remote sensing of tropospheric ozone. *Journal of Quantitative Spectroscopy and Radiative Transfer*, 84(2), 169–179.
- Jusoff, K., & Pathan, M. (2009). Mapping of individual oil palm trees using airborne hyperspectral sensing: an overview. *Applied Physics Research*, 1(1), 15–30.
- Key, T., T.A. Warner., J.B. McGraw & M. A .Fajvan. 2001. A comparison of multispectral and multitemporal information in high spatial resolution imagery for classification of individual tree species in a temperate hardwood forest. *Remote Sensing*, 75, 100–112
- Li, H., Lee, W. S., Wang, K., Ehsani, R., & Yang, C. (2014). “Extended spectral angle mapping (ESAM)” for citrus greening disease detection using airborne hyperspectral imaging. *Precision Agriculture*, 15(2), 162–183.
- López- López, M., Calderón, R., González-Dugo, V., Zarco-Tejada, P. J. & Fereres, E. (2016). Early detection and quantification of almond red leaf blotch using high-resolution hyperspectral and thermal imagery. *Remote Sensing*, 2016, 8(4), 276. <https://doi.org/10.3390/rs8040276>
- Lucieer, A., Malenovský, Z., Veness, T., & Wallace, L. (2014). HyperUAS - Imaging spectroscopy from a multirotor unmanned aircraft system. *Journal of Field Robotics*, 31(4), 571–590.
- Mahlein, A.-K., Steiner, U., Dehne, H.-W., & Oerke, E.-C. (2010). Spectral signatures of sugar beet leaves for the detection and differentiation of diseases. *Precision Agriculture*, 11(4), 413–431.
- Majidi Heravan, E., Davoudi, D., & Khoush Kam, S. (2002). Some morphological and anatomical aspects of Date palm (*Phoenix Dactylifera* L.) somatic embryogenesis in tissue culture. *Journal of Agricultural science and technology(Jast)*, 4(1–2), 63–71.

- Mäkynen, J., Holmlund, C., Saari, H., Ojala, K. & Antila, T. (2011). Unmanned aerial vehicle (UAV) operated megapixel spectral camera. *Electro-Optical Remote Sensing, Photonic Technologies, and Applications V*, 81860Y. <https://doi.org/10.1117/12.897712>
- Mountrakis, G., Im, J., & Ogole, C. (2011). Support vector machines in remote sensing: A review. *ISPRS Journal of Photogrammetry and Remote Sensing*, 66(3), 247–259.
- Näsi, R., Honkavaara, E., Lyytikäinen-Saarenmaa, P., Blomqvist, M., Litkey, P., Hakala, T., Viljanen, N., Kantola, T., Tanhuanpää, T., & Holopainen, M. (2015). Using UAV-based photogrammetry and hyperspectral imaging for mapping bark beetle damage at tree-level. *Remote Sensing*, 7(11), 15467–15493.
- Nilsson, H. (1995). Remote sensing and image analysis in plant pathology. *Annual Review of Phytopathology*, 33(1), 489–528.
- Nixon, R. W. (1950). Imported varieties of dates in the United States. U.S. Department of Agriculture, 834, 138–141
- Rajabi, R., & Ghassemian, H. (2015). Spectral unmixing of hyperspectral imagery using multilayer NMF. *IEEE Geoscience Remote Sensing Letters*, 12(1), 38–42
- Sandmeier, S., Müller, C., Hosgood, B., & Andreoli, G. (1998). Physical mechanisms in hyperspectral BRDF data of grass and watercress. *Remote Sensing of Environment*, 66(2), 222–233.
- Sankaran, S., Maja, J. M., Buchanon, S., & Ehsani, R. (2013). Huanglongbing (Citrus Greening) detection using visible, near infrared and thermal imaging techniques. *Sensors (Switzerland)*, 13(2), 2117–2130.
- Serranti, S., Cesare, D., & Bonifazi, G. (2013). The development of a hyperspectral imaging method for the detection of Fusarium-damaged, yellow berry and vitreous Italian durum wheat kernels. *Biosystems Engineering*, 115(1), 20–30.
- Shen, X., & Cao, L. (2017). Tree-species classification in subtropical forests using airborne hyperspectral and LiDAR data. *Remote Sensing*, 9(11), 1180. <https://doi.org/10.3390/rs9111180>
- Siddiq, M., & Greiby, I. (2014). Overview of date fruit production, postharvest handling, processing, and nutrition. In book: *Dates: Postharvest Science, Processing Technology and Health Benefits*, 1–28. <https://doi.org/10.1002/9781118292419.ch1>

- Soroker, V., Suma, P., Pergola, A. la, Cohen, Y., Cohen, Y., Alchanatis, V., Golomb, O., Goldshtein, E., Hetzroni, A., Galazan, L., Kontodimas, D., Pontikakos, C., Zorovic, M., & Brandstetter, M. (2013). Early detection and monitoring of red palm weevil: approaches and challenges. In *Colloque méditerranéen sur les ravageurs des palmiers*, Nice, France, 16-18 Janvier 2013. Association Française de Protection des Plantes (AFPP).
- Stringer, L. C. (2009). Reviewing the links between desertification and food insecurity: from parallel challenges to synergistic solutions. *Food Security*, 1(2), 113–126.
- Suomalainen, J., Anders, N., Iqbal, S., Roerink, G., Franke, J., Wenting, P., Hänniger, D., Bartholomeus, H., Becker, R., & Kooistra, L. (2014). A lightweight hyperspectral mapping system and photogrammetric processing chain for unmanned aerial vehicles. *Remote Sensing*, 6(11), 11013–11030.
- Tarabalka, Y., Chanussot, J., & Benediktsson, J. A. (2010). Segmentation and classification of hyperspectral images using watershed transformation. *Journal Pattern Recognition*, 43(7), 2367–2379.
- Teena, M., Manickavasagan, A., Mothershaw, A., El Hadi, S., & Jayas, D. S. (2013). Potential of machine vision techniques for detecting fecal and microbial contamination of food products: A review. *Food and Bioprocess Technology*, 6(7), 1621–1634.
- Tengberg, M. (2012). Beginnings and early history of date palm garden cultivation in the Middle East. *Journal of Arid Environments*, 86, 139–147.
- Thenkabail, P. S., Gamage, M. S. D. N., & Smakhtin, V. U. (2004). The use of remote sensing data for drought assessment and monitoring in southwest asia, research report 85, international water management institute.
- Wang, L., & Zhao, C. (2016). Basic theory and main processing techniques of hyperspectral remote sensing. In book: *Hyperspectral Image Processing*, 1–44. 10.1007/978-3-662-47456-3\_1.
- Yao, H., Hruska, Z., Kincaid, R., Brown, R. L., Bhatnagar, D., & Cleveland, T. E. (2013). Detecting maize inoculated with toxigenic and atoxigenic fungal strains with fluorescence hyperspectral imagery. *Biosystems Engineering*, 115(2), 125–135.
- Zarco-Tejada, P. J., Berjón, A., López-Lozano, R., Miller, J. R., Martín, P., Cachorro, V., González, M. R., & De Frutos, A. (2005). Assessing vineyard condition with hyperspectral indices: Leaf and canopy reflectance simulation in a row-structured discontinuous canopy. *Remote Sensing of Environment*, 99(3), 271–287.



Zarco-Tejada, P. J., González-Dugo, V., & Berni, J. A. J. (2012). Fluorescence, temperature and narrow-band indices acquired from a UAV platform for water stress detection using a micro-hyperspectral imager and a thermal camera. *Remote Sensing of Environment*, 117, 322–337.

## Appendices

Appendix 1: Reflectance, Frequency, and Cumulative Percentage of the Barhi, Khadrawi, Khenaizi, Khalas, RedFard and Helali

<i>Barhi</i>	<i>Reflectance</i>	<i>Frequency</i>	<i>Cumulative %</i>	<i>Reflectance</i>	<i>Frequency</i>	<i>Cumulative %</i>
	0.329974	1	0.51	0.822814071	49	25
	0.374777643	12	6.63	0.778010429	26	38.27
	0.419581286	14	13.78	0.598795857	17	46.94
	0.464384929	8	17.86	0.867617714	16	55.10
	0.509188571	7	21.43	0.419581286	14	62.24
	0.553992214	8	25.51	0.374777643	12	68.37
	0.598795857	17	34.18	0.912421357	12	74.49
	0.6435995	10	39.29	0.6435995	10	79.59
	0.688403143	5	41.84	0.464384929	8	83.67
	0.733206786	7	45.41	0.553992214	8	87.76
	0.778010429	26	58.67	0.509188571	7	91.33
	0.822814071	49	83.67	0.733206786	7	94.90
	0.867617714	16	91.84	0.688403143	5	97.45
	0.912421357	12	97.96	More	4	99.49
	More	4	100.00	0.329974	1	100.00
<i>khenaizi</i>	<i>Reflectance</i>	<i>Frequency</i>	<i>Cumulative %</i>	<i>Reflectance</i>	<i>Frequency</i>	<i>Cumulative %</i>
	0.330217	1	0.51	0.823068857	64	32.65
	0.375021714	12	6.63	0.599045286	16	40.82
	0.419826429	14	13.78	0.867873571	16	48.98
	0.464631143	8	17.86	0.419826429	14	56.12
	0.509435857	7	21.43	0.912678286	13	62.76
	0.554240571	8	25.51	0.375021714	12	68.88
	0.599045286	16	33.67	0.64385	11	74.49

Appendix 1: Reflectance, Frequency, and Cumulative percentage of the Barhi, Khadrawi, Khenaizi, Khalas, RedFard and Helali (continued)

<i>khenaizi</i>	<i>Reflectance</i>	<i>Frequency</i>	<i>Cumulative %</i>	<i>Reflectance</i>	<i>Frequency</i>	<i>Cumulative %</i>
	0.64385	11	39.29	0.778264143	11	80.10
	0.688654714	5	41.84	0.464631143	8	84.18
	0.733459429	6	44.90	0.554240571	8	88.27
	0.778264143	11	50.51	0.509435857	7	91.84
	0.823068857	64	83.16	0.733459429	6	94.90
	0.867873571	16	91.33	0.688654714	5	97.45
	0.912678286	13	97.96	More	4	99.49
	More	4	100.00	0.330217	1	100.00
<i>khalas</i>	<i>Reflectance</i>	<i>Frequency</i>	<i>Cumulative %</i>	<i>Reflectance</i>	<i>Frequency</i>	<i>Cumulative %</i>
	0.310582	1	0.51	0.770903429	59	30.10
	0.356614143	12	6.63	0.862967714	16	38.27
	0.402646286	15	14.29	0.402646286	15	45.92
	0.448678429	8	18.37	0.816935571	15	53.57
	0.494710571	7	21.94	0.586774857	14	60.71
	0.540742714	12	28.06	0.356614143	12	66.84
	0.586774857	14	35.20	0.540742714	12	72.96
	0.632807	9	39.80	0.908999857	11	78.57
	0.678839143	6	42.86	0.632807	9	83.16
	0.724871286	7	46.43	0.448678429	8	87.24
	0.770903429	59	76.53	0.494710571	7	90.82
	0.816935571	15	84.18	0.724871286	7	94.39
	0.862967714	16	92.35	0.678839143	6	97.45
	0.908999857	11	97.96	More	4	99.49
	More	4	100.00	0.310582	1	100.00

Appendix 1: Reflectance, Frequency, and Cumulative percentage of the Barhi, Khadrawi, Khenazi, Khalas, RedFard and Helali (continued)

<i>khadrawi</i>	<i>Reflectance</i>	<i>Frequency</i>	<i>Cumulative %</i>	<i>Reflectance</i>	<i>Frequency</i>	<i>Cumulative %</i>
<i>khadwri Fard</i>	0.364221	1	0.51	0.830062357	50	25.51
	0.406570214	10	5.61	0.872411571	31	41.33
	0.448919429	12	11.73	0.618316286	18	50.51
	0.491268643	6	14.8	0.914760786	16	58.67
	0.533617857	7	18.37	0.6606655	13	65.31
	0.575967071	7	21.94	0.448919429	12	71.43
	0.618316286	18	31.12	0.406570214	10	76.53
	0.6606655	13	37.76	0.787713143	10	81.63
	0.703014714	5	40.31	0.533617857	7	85.20
	0.745363929	6	43.37	0.575967071	7	88.78
	0.787713143	10	48.47	0.491268643	6	91.84
	0.830062357	50	73.98	0.745363929	6	94.90
	0.872411571	31	89.80	0.703014714	5	97.45
	0.914760786	16	97.96	More	4	99.49
	More	4	100.00	0.364221	1	100.00
	<i>Reflectance</i>	<i>Frequency</i>	<i>Cumulative %</i>	<i>Reflectance</i>	<i>Frequency</i>	<i>Cumulative %</i>
<i>Fard</i>	0.364221	1	0.51	0.830062357	50	25.51
<i>Fard Helali</i>	0.406570214	10	5.61	0.872411571	31	41.33
	0.448919429	12	11.73	0.618316286	18	50.51
	0.491268643	6	14.80	0.914760786	16	58.67
	0.533617857	7	18.37	0.6606655	13	65.31
	0.575967071	7	21.94	0.448919429	12	71.43
	0.618316286	18	31.12	0.406570214	10	76.53
	0.6606655	13	37.76	0.787713143	10	81.63
	0.703014714	5	40.31	0.533617857	7	85.20

Appendix 1: Reflectance, Frequency, and Cumulative percentage of the Barhi, Khadrawi, Khenazi, Khalas, RedFard and Helali (continued)

<i>Fard</i>	<i>Reflectance</i>	<i>Frequency</i>	<i>Cumulative %</i>	<i>Reflectance</i>	<i>Frequency</i>	<i>Cumulative %</i>
<i>Helali</i>						
	0.745363929	6	43.37	0.575967071	7	88.78
	0.787713143	10	48.47	0.491268643	6	91.84
	0.830062357	50	73.98	0.745363929	6	94.90
	0.872411571	31	89.80	0.703014714	5	97.45
	0.914760786	16	97.96	More	4	99.49
	More	4	100.00	0.364221	1	100.00
	<i>Reflectance</i>	<i>Frequency</i>	<i>Cumulative %</i>	<i>Reflectance</i>	<i>Frequency</i>	<i>Cumulative %</i>
<i>Helali</i>	0.341369	1	0.51	0.824555	64	32.65
<i>Helali</i>	0.385295	12	6.63	0.604925	18	41.84
	0.429221	14	13.78	0.868481	17	50.51
	0.473147	6	16.84	0.429221	14	57.65
	0.517073	7	20.41	0.912407	13	64.29
	0.560999	8	24.49	0.385295	12	70.41
	0.604925	18	33.67	0.780629	11	76.02
	0.648851	10	38.78	0.648851	10	81.12
	0.692777	5	41.33	0.560999	8	85.20
	0.736703	6	44.39	0.517073	7	88.78
	0.780629	11	50.00	0.473147	6	91.84
	0.824555	64	82.65	0.736703	6	94.90
	0.868481	17	91.33	0.692777	5	97.45
	0.912407	13	97.96	More	4	99.49
	More	4	100.00	0.341369	1	100.00

Appendix 2: Statistic Reading of the Barhi, Khadrawi, Khenaizi, Khalas, RedFard and Helali

<i>Standard Deviation</i>	<i>Sample Variance</i>	<i>Barhi</i>	<i>Khalas</i>	<i>Khenaizi</i>	<i>Kadrawi</i>	<i>Fard</i>	<i>Helali</i>	<i>NM</i>
0.001931987	3.73257E-06	0.956632	0.96152	0.956051	0.958872	0.957998	0.95792	395.35
0.001200738	1.44177E-06	0.945962	0.948558	0.944886	0.946534	0.946194	0.946542	398.34
0.001478609	2.18628E-06	0.934779	0.938333	0.93406	0.936479	0.935964	0.935724	401.33
0.001782391	3.17692E-06	0.921104	0.925202	0.919827	0.922244	0.922355	0.921961	404.33
0.001860755	3.46241E-06	0.910272	0.913864	0.908551	0.912064	0.911132	0.909796	407.32
0.00158574	2.51457E-06	0.898359	0.902012	0.89749	0.90021	0.900231	0.899546	410.32
0.001877654	3.52558E-06	0.895835	0.898529	0.89317	0.896098	0.897347	0.894826	413.32
0.001251143	1.56536E-06	0.876754	0.878759	0.875664	0.876475	0.878579	0.876535	416.32
0.001568888	2.46141E-06	0.881815	0.884098	0.880604	0.882246	0.884508	0.881221	419.32
0.001526125	2.32906E-06	0.864005	0.867384	0.863681	0.865297	0.866721	0.864293	422.33
0.001249864	1.56216E-06	0.853299	0.855523	0.853369	0.85301	0.855764	0.853279	425.33
0.001268128	1.60815E-06	0.857958	0.860283	0.857416	0.858369	0.860065	0.857507	428.34
0.00145412	2.11447E-06	0.818921	0.822033	0.819134	0.819597	0.821771	0.818884	431.35
0.001811033	3.27984E-06	0.816594	0.820068	0.815848	0.816951	0.819164	0.815694	434.36
0.002167843	4.69954E-06	0.793018	0.797242	0.792586	0.793694	0.797119	0.792873	437.37
0.001912788	3.65876E-06	0.778557	0.782251	0.779575	0.779392	0.783228	0.77906	440.38
0.001928669	3.71976E-06	0.769883	0.774152	0.770309	0.770335	0.773623	0.770192	443.4
0.002139387	4.57698E-06	0.754681	0.759153	0.754782	0.754739	0.758474	0.754573	446.42
0.002599384	6.7568E-06	0.761258	0.766265	0.760585	0.761695	0.765627	0.760473	449.43
0.002482362	6.16212E-06	0.731207	0.736499	0.731004	0.731245	0.735576	0.731674	452.45
0.002332065	5.43853E-06	0.744995	0.749444	0.744652	0.744242	0.748517	0.744245	455.47
0.003188982	1.01696E-05	0.738295	0.744374	0.735989	0.738797	0.741905	0.736827	458.5

Appendix 2: Statistic Reading of the Barhi, Khadrawi, Khenaizi, Khalas, RedFard and Helali (continued)

<i>Standard Deviation</i>	<i>Sample Variance</i>	<i>Barhi</i>	<i>Khalas</i>	<i>Khenaizi</i>	<i>Kadrawi</i>	<i>Fard</i>	<i>Helali</i>	<i>NM</i>
0.002469362	6.09775E-06	0.700353	0.705139	0.69976	0.698847	0.703522	0.700063	461.52
0.002269241	5.14946E-06	0.738869	0.743803	0.739152	0.737878	0.741631	0.738542	464.55
0.002975598	8.85418E-06	0.718909	0.724444	0.717292	0.720096	0.723314	0.717656	467.57
0.002882682	8.30986E-06	0.670067	0.675978	0.669814	0.66906	0.674603	0.67042	470.6
0.002626348	6.8977E-06	0.699865	0.704716	0.700273	0.697271	0.703182	0.700553	473.63
0.003232576	1.04495E-05	0.671621	0.678429	0.670144	0.672551	0.675556	0.670531	476.66
0.003305119	1.09238E-05	0.624795	0.631748	0.62399	0.623466	0.62911	0.625101	479.7
0.003239419	1.04938E-05	0.645396	0.651737	0.645299	0.642866	0.649687	0.646445	482.73
0.003469461	1.20372E-05	0.622281	0.629731	0.620518	0.622074	0.626657	0.622778	485.77
0.003817245	1.45714E-05	0.586935	0.5951	0.584971	0.585877	0.591295	0.588272	488.8
0.003794257	1.43964E-05	0.595033	0.60357	0.593365	0.594103	0.598785	0.596533	491.84
0.004449375	1.97969E-05	0.576937	0.586705	0.574049	0.576067	0.580522	0.578654	494.88
0.004626177	2.14015E-05	0.577857	0.587446	0.575339	0.574802	0.580795	0.579962	497.93
0.004706499	2.21511E-05	0.603376	0.613381	0.599394	0.602575	0.605589	0.604247	500.97
0.006080869	3.6977E-05	0.569549	0.581822	0.563177	0.568873	0.570974	0.571003	504.02
0.007029119	4.94085E-05	0.558111	0.571367	0.552205	0.55254	0.558769	0.561317	507.06
0.006805328	4.63125E-05	0.608016	0.620661	0.601327	0.603101	0.607288	0.609724	510.11
0.008216416	6.75095E-05	0.599677	0.613859	0.588893	0.595564	0.597466	0.5989	513.16
0.010257027	0.000105207	0.561093	0.578856	0.549179	0.553817	0.557048	0.562509	516.21
0.010334658	0.000106805	0.59305	0.608737	0.580485	0.581611	0.58779	0.593512	519.27
0.010756988	0.000115713	0.619894	0.636451	0.604961	0.611379	0.613074	0.61729	522.32
0.013539542	0.000183319	0.578042	0.597777	0.557536	0.567686	0.569128	0.573484	525.38

Appendix 2: Statistic Reading of the Barhi, Khadrawi, Khenaizi, Khalas, RedFard and Helali (continued)

<i>Standard Deviation</i>	<i>Sample Variance</i>	<i>Barhi</i>	<i>Khalas</i>	<i>Khenaizi</i>	<i>Kadrawi</i>	<i>Fard</i>	<i>Helali</i>	<i>NM</i>
0.014460428	0.000209104	0.560857	0.581524	0.540383	0.545974	0.550898	0.556145	528.43
0.013273442	0.000176184	0.601942	0.619929	0.583246	0.586138	0.592138	0.595919	531.49
0.013831208	0.000191302	0.607229	0.62557	0.585754	0.594271	0.596556	0.596929	534.55
0.015931126	0.000253801	0.565645	0.586756	0.540606	0.551396	0.553767	0.553349	537.62
0.016435539	0.000270127	0.553528	0.575008	0.528324	0.53673	0.540833	0.540752	540.68
0.016086093	0.000258762	0.566263	0.58608	0.540386	0.549246	0.553031	0.552953	543.74
0.017477528	0.000305464	0.551154	0.572563	0.521849	0.534666	0.536715	0.537261	546.81
0.01782057	0.000317573	0.537311	0.559971	0.508683	0.519913	0.52266	0.524064	549.88
0.017269313	0.000298229	0.546599	0.568324	0.518782	0.528948	0.532451	0.534024	552.95
0.017337129	0.000300576	0.549743	0.571767	0.52151	0.533336	0.535682	0.53717	556.02
0.018005681	0.000324205	0.528415	0.550895	0.498739	0.51081	0.513306	0.516141	559.09
0.01768682	0.000312824	0.521423	0.544165	0.493754	0.502832	0.506328	0.511005	562.17
0.016829358	0.000283227	0.53729	0.558901	0.510786	0.519784	0.523322	0.526625	565.24
0.017053472	0.000290821	0.52974	0.552504	0.502433	0.515351	0.516906	0.518452	568.32
0.017524435	0.000307106	0.498081	0.521909	0.470656	0.482734	0.484715	0.488115	571.4
0.016593085	0.00027533	0.490113	0.513259	0.466175	0.472915	0.477478	0.483741	574.48
0.014794965	0.000218891	0.51697	0.537537	0.496081	0.500684	0.505885	0.5121	577.56
0.014534091	0.00021124	0.521739	0.542293	0.499456	0.509516	0.511833	0.514915	580.65
0.016315138	0.000266184	0.48183	0.505275	0.456346	0.470515	0.471071	0.474731	583.73
0.016281096	0.000265074	0.447659	0.472319	0.424879	0.433952	0.437388	0.445011	586.82



Appendix 2: Statistic Reading of the Barhi, Khadrawi, Khenaizi, Khalas, RedFard and Helali (continued)

<i>Standard Deviation</i>	<i>Sample Variance</i>	<i>Barhi</i>	<i>Khalas</i>	<i>Khenaizi</i>	<i>Kadrawi</i>	<i>Fard</i>	<i>Helali</i>	<i>NM</i>
0.015138877	0.000229186	0.459675	0.482116	0.440834	0.442985	0.450143	0.460084	589.91
0.013795313	0.000190311	0.489717	0.510619	0.471892	0.475726	0.481344	0.488422	593
0.014374467	0.000206625	0.482835	0.504882	0.461985	0.472337	0.475112	0.4787	596.09
0.015589175	0.000243022	0.447926	0.472417	0.425715	0.437594	0.439726	0.44369	599.18
0.015368693	0.000236197	0.429204	0.453968	0.409494	0.416431	0.421175	0.427269	602.28
0.014222537	0.000202281	0.443324	0.466293	0.427026	0.428983	0.4359	0.442199	605.37
0.013648617	0.000186285	0.45468	0.476387	0.437159	0.442583	0.447398	0.451409	608.47
0.014505085	0.000210397	0.43335	0.456445	0.413336	0.423175	0.426187	0.428346	611.57
0.014839124	0.0002202	0.403374	0.427864	0.383625	0.393844	0.396789	0.399232	614.67
0.014552511	0.000211776	0.390893	0.415577	0.372982	0.380369	0.384773	0.388668	617.77
0.013801896	0.000190492	0.396837	0.420476	0.380772	0.38589	0.391223	0.39571	620.87
0.013519935	0.000182789	0.400248	0.423409	0.3839	0.390468	0.394979	0.399302	623.98
0.013630742	0.000185797	0.390736	0.414217	0.373977	0.381572	0.385926	0.389734	627.09
0.013810696	0.000190735	0.381028	0.405374	0.364882	0.37193	0.376267	0.381106	630.19
0.013631163	0.000185809	0.38285	0.406847	0.366845	0.373762	0.378589	0.383335	633.3
0.013076708	0.000171	0.385466	0.408765	0.370133	0.377378	0.381869	0.38605	636.42
0.012648002	0.000159972	0.376283	0.399468	0.361663	0.369707	0.374149	0.37722	639.53
0.012069504	0.000145673	0.359591	0.382667	0.34673	0.353984	0.359193	0.362132	642.64
0.011083486	0.000122844	0.353441	0.375515	0.343517	0.347744	0.355044	0.357829	645.76
0.009796751	9.59763E-05	0.365773	0.385761	0.358059	0.360602	0.36874	0.370378	648.88

Appendix 2: Statistic Reading of the Barhi, Khadrawi, Khenaizi, Khalas, RedFard and Helali (continued)

<i>Standard Deviation</i>	<i>Sample Variance</i>	<i>Barhi</i>	<i>Khalas</i>	<i>Khenaizi</i>	<i>Kadrawi</i>	<i>Fard</i>	<i>Helali</i>	<i>NM</i>
0.008899825	7.92069E-05	0.381072	0.399405	0.373575	0.377322	0.384475	0.383501	651.99
0.008843416	7.8206E-05	0.377725	0.39608	0.369645	0.376616	0.381729	0.377617	655.11
0.008947468	8.00572E-05	0.353262	0.372524	0.345946	0.353604	0.358349	0.353252	658.24
0.0083236	6.92823E-05	0.33083	0.349635	0.325482	0.331072	0.337306	0.332789	661.36
0.007416471	5.5004E-05	0.327765	0.345252	0.325111	0.327416	0.335642	0.332102	664.49
0.006571569	4.31855E-05	0.342382	0.358165	0.341372	0.342563	0.351323	0.34699	667.61
0.006230948	3.88247E-05	0.356892	0.371915	0.355943	0.358407	0.366331	0.360591	670.74
0.006292728	3.95984E-05	0.35522	0.370169	0.353665	0.358316	0.365233	0.358708	673.87
0.006578899	4.32819E-05	0.340108	0.35608	0.338495	0.344204	0.350447	0.344857	677
0.006674234	4.45454E-05	0.327973	0.344692	0.327615	0.331679	0.338824	0.335983	680.13
0.0072955	5.32243E-05	0.333194	0.35133	0.333542	0.335388	0.343354	0.344167	683.27
0.008214671	6.74808E-05	0.356758	0.375623	0.355053	0.356503	0.364129	0.368719	686.4
0.010197988	0.000103999	0.382029	0.403146	0.375169	0.379193	0.384556	0.392679	689.54
0.014016887	0.000196473	0.397818	0.422646	0.382177	0.391067	0.393423	0.405709	692.68
0.018938769	0.000358677	0.405505	0.435018	0.380311	0.393135	0.393418	0.410618	695.82
0.023534726	0.000553883	0.419746	0.451152	0.383798	0.400079	0.399135	0.42064	698.96
0.026183801	0.000685591	0.447108	0.478404	0.404046	0.422004	0.420947	0.443935	702.1
0.026633977	0.000709369	0.485868	0.514393	0.4388	0.457729	0.457551	0.478543	705.25
0.025625812	0.000656682	0.526606	0.5519	0.478741	0.498218	0.499178	0.516216	708.4
0.023500951	0.000552295	0.563059	0.584754	0.516743	0.536859	0.539209	0.550698	711.54
0.021044789	0.000442883	0.592322	0.610618	0.548708	0.569637	0.573387	0.57817	714.69
0.018070757	0.000326552	0.615601	0.630636	0.576941	0.597282	0.602959	0.60079	717.84
0.014871197	0.000221152	0.635992	0.648286	0.604488	0.622905	0.630854	0.621179	721

Appendix 2: Statistic Reading of the Barhi, Khadrawi, Khenaizi, Khalas, RedFard and Helali (continued)

<i>Standard Deviation</i>	<i>Sample Variance</i>	<i>Barhi</i>	<i>Khalas</i>	<i>Khenaizi</i>	<i>Kadrawi</i>	<i>Fard</i>	<i>Helali</i>	<i>NM</i>
0.012063419	0.000145526	0.65582	0.665668	0.632458	0.648211	0.658607	0.641968	724.15
0.010078247	0.000101571	0.674639	0.681935	0.66048	0.672436	0.685287	0.662161	727.31
0.00996505	9.93022E-05	0.691278	0.696846	0.685987	0.694786	0.709564	0.680662	730.46
0.011207268	0.000125603	0.704667	0.708717	0.707792	0.712922	0.72978	0.696098	733.62
0.013135786	0.000172549	0.714922	0.717921	0.725722	0.727829	0.746178	0.708665	736.78
0.015175768	0.000230304	0.722906	0.725274	0.740128	0.739536	0.759406	0.718535	739.94
0.01701059	0.00028936	0.729933	0.731256	0.752492	0.749625	0.770621	0.727409	743.11
0.01859111	0.000345629	0.735573	0.736439	0.762736	0.757856	0.779861	0.734853	746.27
0.020015402	0.000400616	0.739943	0.740118	0.770616	0.764489	0.787514	0.74103	749.44
0.021347429	0.000455713	0.741861	0.741305	0.775835	0.768608	0.792276	0.744611	752.61
0.022296275	0.000497124	0.742492	0.741894	0.779206	0.770375	0.795273	0.746825	755.78
0.022842962	0.000521801	0.742806	0.742616	0.78127	0.771952	0.797391	0.748958	758.95
0.023168386	0.000536774	0.744511	0.744104	0.784422	0.773918	0.799768	0.751809	762.12
0.023137218	0.000535331	0.747956	0.746848	0.788256	0.776704	0.802958	0.7562	765.29
0.023115892	0.000534344	0.751063	0.750738	0.791498	0.780793	0.806782	0.760638	768.47
0.023156231	0.000536211	0.754344	0.75301	0.794074	0.783697	0.809958	0.763918	771.65
0.023222334	0.000539277	0.755222	0.753916	0.795134	0.785132	0.811061	0.765317	774.83
0.023400724	0.000547594	0.753105	0.752366	0.793848	0.784278	0.809753	0.764619	778.01
0.023894215	0.000570934	0.750442	0.749727	0.792105	0.782044	0.808557	0.76285	781.19
0.024075817	0.000579645	0.749254	0.74864	0.791915	0.78082	0.807832	0.762502	784.37
0.023842445	0.000568462	0.75074	0.750737	0.793582	0.781828	0.809078	0.764423	787.56
0.023323467	0.000543984	0.755691	0.755733	0.797768	0.785619	0.812957	0.769617	790.74

Appendix 2: Statistic Reading of the Barhi, Khadrawi, Khenaizi, Khalas, RedFard and Helali (continued)

<i>Standard Deviation</i>	<i>Sample Variance</i>	<i>Barhi</i>	<i>Khalas</i>	<i>Khenaizi</i>	<i>Kadrawi</i>	<i>Fard</i>	<i>Helali</i>	<i>NM</i>
0.022588724	0.00051025	0.761903	0.761432	0.802362	0.790872	0.81715	0.77536	793.93
0.022060891	0.000486683	0.766106	0.766066	0.80575	0.794874	0.8203	0.779574	797.12
0.022015686	0.00048469	0.766442	0.766658	0.806165	0.795964	0.820529	0.780123	800.31
0.022222219	0.000493827	0.764276	0.764643	0.8042	0.794198	0.819079	0.778206	803.5
0.022574465	0.000509606	0.759805	0.760521	0.800372	0.790383	0.815782	0.774314	806.7
0.022876877	0.000523351	0.755202	0.756335	0.796679	0.786697	0.812117	0.77061	809.89
0.023118129	0.000534448	0.752562	0.753633	0.794757	0.783955	0.810086	0.768571	813.09
0.022878139	0.000523409	0.752794	0.754377	0.795343	0.784007	0.809905	0.769665	816.29
0.022714729	0.000515959	0.755406	0.756598	0.797596	0.786129	0.811983	0.772438	819.49
0.022299734	0.000497278	0.759214	0.760694	0.800705	0.789214	0.815003	0.776059	822.69
0.022041629	0.000485833	0.762581	0.764346	0.804021	0.792255	0.817811	0.779699	825.89
0.02194149	0.000481429	0.764306	0.76601	0.805286	0.793851	0.819365	0.781213	829.1
0.021814921	0.000475891	0.764558	0.766506	0.805291	0.794469	0.819469	0.781716	832.3
0.021924335	0.000480676	0.763295	0.765408	0.804426	0.793699	0.818423	0.780543	835.51
0.022298105	0.000497205	0.76113	0.763337	0.802801	0.791906	0.817433	0.779019	838.72
0.022523041	0.000507287	0.759726	0.76204	0.801996	0.790949	0.816579	0.777993	841.93
0.022604734	0.000510974	0.759587	0.761867	0.802377	0.790769	0.816501	0.778185	845.14
0.022553598	0.000508665	0.760706	0.762978	0.803244	0.791629	0.817598	0.779209	848.36
0.022389365	0.000501284	0.762813	0.765357	0.805296	0.793484	0.819449	0.781592	851.57
0.022322056	0.000498274	0.76541	0.767686	0.807877	0.795685	0.821644	0.783967	854.79
0.021858069	0.000477775	0.768302	0.771006	0.810312	0.798328	0.823553	0.787199	858.01
0.021638563	0.000468227	0.770745	0.773724	0.812478	0.800622	0.82553	0.789344	861.23

Appendix 2: Statistic Reading of the Barhi, Khadrawi, Khenaizi, Khalas, RedFard and Helali (continued)

<i>Standard Deviation</i>	<i>Sample Variance</i>	<i>Barhi</i>	<i>Khalas</i>	<i>Khenaizi</i>	<i>Kadrawi</i>	<i>Fard</i>	<i>Helali</i>	<i>NM</i>
0.021418392	0.000458748	0.772156	0.775293	0.81371	0.801975	0.826275	0.790276	864.45
0.021263049	0.000452117	0.772718	0.776625	0.814289	0.80303	0.826794	0.791167	867.67
0.02123636	0.000450983	0.772836	0.777164	0.814485	0.803169	0.827018	0.791081	870.9
0.02118745	0.000448908	0.772714	0.776491	0.813958	0.802915	0.826451	0.790343	874.12
0.020994345	0.000440763	0.771314	0.775685	0.812317	0.801211	0.824933	0.78881	877.35
0.020873931	0.000435721	0.769367	0.774431	0.810391	0.799381	0.822957	0.786731	880.58
0.020880422	0.000435992	0.767756	0.772836	0.808908	0.797531	0.821373	0.785209	883.81
0.020705072	0.0004287	0.766979	0.772514	0.808544	0.79702	0.820069	0.784811	887.04
0.020395969	0.000415996	0.76801	0.773768	0.809112	0.797526	0.820407	0.785472	890.28
0.020060928	0.000402441	0.768958	0.774873	0.809761	0.797715	0.820528	0.786318	893.51
0.019402068	0.00037644	0.769625	0.776177	0.809731	0.797542	0.819664	0.786554	896.75
0.018667682	0.000348482	0.768828	0.776915	0.80856	0.796305	0.817288	0.785227	899.99
0.018026768	0.000324964	0.76823	0.777547	0.80748	0.795052	0.815204	0.783802	903.23
0.016995014	0.000288831	0.766866	0.776576	0.80522	0.792946	0.810737	0.782018	906.47
0.016619603	0.000276211	0.764636	0.775586	0.802727	0.790648	0.807913	0.779739	909.71
0.016352225	0.000267395	0.763913	0.775157	0.801355	0.789766	0.806634	0.778522	912.95
0.016296481	0.000265575	0.76467	0.775859	0.801779	0.790693	0.80728	0.779065	916.2
0.016415646	0.000269473	0.765227	0.776236	0.802333	0.791206	0.808293	0.779826	919.45
0.016421044	0.000269651	0.766714	0.777738	0.80414	0.792701	0.809669	0.781585	922.7
0.016455204	0.000270774	0.769533	0.779924	0.806834	0.795203	0.812444	0.784437	925.95
0.01605222	0.000257674	0.774228	0.784493	0.810647	0.798717	0.816394	0.789297	929.2

Appendix 2: Statistic Reading of the Barhi, Khadrawi, Khenazi, Khalas, RedFard and Helali (continued)

<i>Standard Deviation</i>	<i>Sample Variance</i>	<i>Barhi</i>	<i>Khalas</i>	<i>Khenazi</i>	<i>Kadrawi</i>	<i>Fard</i>	<i>Helali</i>	<i>NM</i>
0.015704504	0.000246631	0.779815	0.790049	0.815825	0.803276	0.821137	0.795164	932.45
0.015233108	0.000232048	0.788089	0.797137	0.822922	0.810118	0.827834	0.802957	935.71
0.014457756	0.000209027	0.798329	0.806186	0.83093	0.818257	0.83594	0.811974	938.97
0.014054185	0.00019752	0.807278	0.814947	0.839016	0.826967	0.843914	0.820996	942.22
0.013895866	0.000193095	0.815411	0.822322	0.846069	0.834664	0.851818	0.82916	945.48
0.013844269	0.000191664	0.821002	0.827375	0.851068	0.839838	0.857435	0.835296	948.75
0.013761873	0.000189389	0.825145	0.830581	0.853682	0.8444	0.861685	0.839855	952.01
0.013729912	0.00018851	0.827057	0.83154	0.854468	0.845074	0.863609	0.841757	955.27
0.013745309	0.000188934	0.826453	0.831526	0.854593	0.844333	0.863088	0.841676	958.54
0.013734782	0.000188644	0.826641	0.83127	0.854343	0.843813	0.863259	0.842315	961.81
0.013733048	0.000188597	0.827292	0.83129	0.854394	0.844483	0.863826	0.843021	965.07
0.013742679	0.000188861	0.828882	0.832925	0.855736	0.845626	0.865597	0.844343	968.35
0.013618628	0.000185467	0.831397	0.836051	0.858883	0.848209	0.867743	0.847041	971.62
0.013192042	0.00017403	0.836279	0.839993	0.862481	0.851736	0.871195	0.851225	974.89
0.0124625	0.000155314	0.841498	0.845178	0.866738	0.856639	0.874323	0.85552	978.17
0.01183677	0.000140109	0.847508	0.851493	0.871826	0.861897	0.878823	0.861195	981.44
0.011221431	0.000125921	0.853836	0.858513	0.87744	0.867424	0.883782	0.867308	984.72
0.010723282	0.000114989	0.859848	0.86427	0.882357	0.873447	0.888448	0.872274	988
0.010134203	0.000102702	0.866246	0.870077	0.887132	0.878706	0.893128	0.876506	991.28
0.009614258	9.2434E-05	0.871468	0.874859	0.891529	0.882932	0.896586	0.880638	994.56
0.008922259	7.96067E-05	0.875173	0.879096	0.893197	0.886622	0.899241	0.883596	997.85
0.008213159	6.7456E-05	0.879175	0.88358	0.89707	0.890415	0.901027	0.887263	1001.13
0.007758742	6.01981E-05	0.882847	0.887221	0.900395	0.893731	0.903092	0.890266	1004.42